

Heavy Quarkonium Production through the Semi-Exclusive e^+e^- Annihilation Channels around the Z^0 Peak

Zhan Sun, Xing-Gang Wu,* Gu Chen, Jun Jiang, and Zhi Yang
Department of Physics, Chongqing University, Chongqing 401331, P.R. China
(Dated: February 7, 2022)

Within the framework of the non-relativistic QCD, we present a detailed discussion on the heavy quarkonium production at the leading order in α_s at a e^+e^- collider with the collision energy around the Z^0 peak. Quarkonia are produced through the semi-exclusive channels $e^+e^- \rightarrow |H_{Q\bar{Q}}\rangle + X$ with $X = Q\bar{Q}$ or gg , where Q indicates a heavy quark (respectively b or c). It is noted that in addition to the color-singlet $1S$ -level quarkonium states, the $2S$ and $1P$ color-singlet states and the color-octet $|(Q\bar{Q})[{}^3S_1^{(8)}]g\rangle$ state also provide sizable contributions. The heavy quarkonium transverse momentum and rapidity distributions for the e^+e^- collision energy $E_{cm} = m_Z$ are presented. For both charmonium and bottomonium production via the Z^0 propagator, there is approximate “spin degeneracy” between the spin-triplet and spin-singlet quarkonium states. Uncertainties for the total cross sections are estimated by taking $m_c = 1.50 \pm 0.15$ GeV and $m_b = 4.90 \pm 0.15$ GeV. Around $E_{cm} = m_Z$, due to the Z^0 -boson resonance effect, total cross sections for the channels via the Z^0 -propagator become much larger than the channels via the virtual photon propagator. We conclude that, in addition to the B factories as BaBar and Belle and the hadronic colliders as Tevatron and LHC, such a super Z -factory will present an excellent platform for studying the heavy quarkonium properties.

PACS numbers: 13.66.Bc, 12.38.Bx, 12.39.Jh

I. INTRODUCTION

The investigation of the heavy quarkonium, e.g. charmonium and bottomonium can help us to achieve a deeper understanding of QCD in both the perturbative and nonperturbative sectors [1–11]. A comprehensive review of heavy quarkonium physics can be found in Ref.[12]. In comparison to the hadronic colliders as Tevatron and LHC, an e^+e^- -collider has many advantages, as it provides a cleaner environment and the collision energy of the incoming electron-positron beams is well under control. Recently, a super Z factory running at an energy around the Z^0 -boson mass with a high luminosity $\mathcal{L} \simeq 10^{34-36} \text{cm}^{-2}\text{s}^{-1}$, similar to the GigaZ program of the Internal Linear Collider [13, 14], has been proposed [15]. In the present paper, we will concentrate our attention on the heavy quarkonium production at such a super Z factory. This can be a useful reference for experimental studies, complementing the present BaBar and Belle results on heavy quarkonia.

The non-relativistic QCD (NRQCD) [16] provides a systematic approach for treating the inclusive decay and production of the heavy quarkonia [16]. In this approach, effects of higher-Fock components of a quarkonium state can be considered systematically. Although the probability to find such higher-Fock components is suppressed, the effects of these higher-Fock states can be very significant. This has been shown in the explanation of the ψ' -anomaly at Tevatron [17], where the inclusive ψ' -production rate with large transverse momentum is in order of magnitude larger than the predicted if one only considers the color-singlet Fock state. By taking the color-octet ($c\bar{c}$) components into account, the Tevatron data can be explained [18]. This is regarded as a great triumph of NRQCD.

Despite many successes of NRQCD, some problems still remain unsolved. Among them a crucial one is that the approach fails to predict the polarization of J/ψ at the large transverse momentum (p_T) measured at Tevatron. The hadronic production of J/ψ is dominated by the gluon fragmentation in which a gluon fragments into a color-octet state ($c\bar{c}$)[${}^3S_1^{(8)}$]. If the spin-symmetry hold for charm quarks, as is usually adopted in the literature, then the prompt J/ψ shall always show large transverse polarization [19]. But this prediction contradicts with the measured at Tevatron [20, 21] and the newly LHC data [22]. This is puzzling because the same mechanism explains the production of unpolarized J/ψ but fails to explain the polarization of the produced J/ψ . On the one hand, this shows that the NRQCD itself could be immature. For example, in Ref.[23] it has pointed out that a spin-flipping effect in the transition from the color-octet ($c\bar{c}$)-pair to the produced J/ψ could cure the polarization puzzle to a certain degree.

*Electronic address: wuxg@cqu.edu.cn

On the other hand, it is helpful to find another platform in addition to the hadronic colliders, such as the cleaner e^+e^- collider, to test NRQCD.

Within the framework of NRQCD, the production process can be factorized into a sum of products of short-distance coefficients and long-distance matrix elements [16]. The short-distance coefficients are perturbatively calculable in a power series of α_s at the energy scale around the heavy quark mass. Generally, the non-perturbative long-distance matrix elements can be determined from lattice QCD calculations, or by fitting the prediction with the experimental data, or be roughly estimated by means of the NRQCD scaling rule. It has been shown that the matching of the color-octet matrix elements from the hadronic experiments strongly depends on the parton distribution function (PDF) [18, 24–28], and the PDF uncertainty usually provides one of the key uncertainties for the theoretical estimations. Regarding this point, the e^+e^- collider provides a better platform for precise studies than the hadronic colliders and for testing the NRQCD formulas.

Within the framework of NRQCD, the physical state of a heavy quarkonium is described as a superposition of Fock states, and the relative importance among those infinite ingredients is evaluated by the velocity scaling rule [16]. When the $(Q\bar{Q})$ -pair preceding the formation of the hadron $|H_{Q\bar{Q}}\rangle$ is in color-singlet state, it usually gives the dominant contribution to the heavy quarkonium productions and decays; while the production via the color-octet $(Q\bar{Q})$ -pair is suppressed by powers of v . Here v stands for the typical velocity of the heavy quark and anti-quark in the quarkonium rest frame, $v^2 \simeq 0.23$ for $(c\bar{c})$ -quarkonium and $v^2 \simeq 0.08$ for $(b\bar{b})$ -quarkonium. For example, in the velocity expansion, we have

$$|\eta_Q\rangle = \mathcal{O}(1)|Q\bar{Q}[^1S_0^{(1)}]\rangle + \mathcal{O}(v)|Q\bar{Q}[^1P_1^{(8)}]g\rangle + \dots, \quad (1)$$

$$|\psi_Q\rangle = \mathcal{O}(1)|Q\bar{Q}[^3S_1^{(1)}]\rangle + \mathcal{O}(v)|Q\bar{Q}[^3P_J^{(8)}]g\rangle + \dots, \quad (2)$$

$$|h_Q\rangle = \mathcal{O}(1)|Q\bar{Q}[^1P_1^{(1)}]\rangle + \mathcal{O}(v)|Q\bar{Q}[^1S_0^{(8)}]g\rangle + \dots, \quad (3)$$

$$|\chi_{QJ}\rangle = \mathcal{O}(1)|Q\bar{Q}[^3P_J^{(1)}]\rangle + \mathcal{O}(v)|Q\bar{Q}[^3S_1^{(8)}]g\rangle + \dots, \quad (4)$$

where $Q = b$ or c . Throughout the paper we denote the pre-quarkonium color-octet and color-singlet $(Q\bar{Q})$ states with the extra superscripts **(8)** and **(1)**, respectively. Later on we omit the superscript **(1)** for the color-singlet case. The angular momentum properties of the Fock states are defined in square brackets. The color-octet $(Q\bar{Q})$ -pair can give sizable and observable contributions in certain cases or in certain kinematic regions when the color-singlet terms are highly suppressed by the hard scattering part. For example, for the B_c meson decaying into leptons and inclusive light hadrons, the energy spectrum of the charged lepton for the color-octet components of the B_c meson is dominant over its color-singlet component when the lepton has high energy [29].

In the present paper, we will make a detailed discussion on the heavy quarkonium production at the super Z factory via the following two semi-exclusive channels: $e^+e^- \rightarrow \gamma^*/Z^0 \rightarrow |H_{Q\bar{Q}}\rangle + Q\bar{Q}$ and $e^+e^- \rightarrow \gamma^*/Z^0 \rightarrow |H_{Q\bar{Q}}\rangle + gg$. At present the BaBar and Belle measurements of these two processes are used to determine the color-octet components. However, the present estimations (especially for the charmonium case) are inconsistent with each other [30–32]. Thus, it would be helpful to find a new platform, such as the super Z factory, to learn more about these processes. More explicitly, we will deal with the following production processes:

$$\begin{aligned} e^+e^- &\rightarrow Z^0, \gamma^* \rightarrow |(Q\bar{Q})[(^1S_1), (^2S_1), (^1S_0), (^2S_0)]\rangle + Q\bar{Q}, \\ e^+e^- &\rightarrow Z^0, \gamma^* \rightarrow |(Q\bar{Q})[(^1P_1), (^1P_0), (^1P_1), (^1P_2)]\rangle + Q\bar{Q}, \\ e^+e^- &\rightarrow Z^0 \rightarrow |(Q\bar{Q})[(^1S_0^{(8)}), (^1S_1^{(8)})]g\rangle + Q\bar{Q} \rightarrow \psi_Q + Q\bar{Q}, \\ e^+e^- &\rightarrow Z^0 \rightarrow |(Q\bar{Q})[(^1S_0^{(8)})]g\rangle + Q\bar{Q} \rightarrow h_Q + Q\bar{Q}, \\ e^+e^- &\rightarrow Z^0 \rightarrow |(Q\bar{Q})[(^1S_1^{(8)})]g\rangle + Q\bar{Q} \rightarrow \chi_{QJ} + Q\bar{Q} \end{aligned}$$

and

$$\begin{aligned} e^+e^- &\rightarrow Z^0, \gamma^* \rightarrow |(Q\bar{Q})[(^1S_1), (^2S_1)]\rangle + gg, \\ e^+e^- &\rightarrow Z^0 \rightarrow |(Q\bar{Q})[(^1S_0), (^2S_0)]\rangle + gg, \\ e^+e^- &\rightarrow Z^0 \rightarrow |(Q\bar{Q})[(^1S_0^{(8)}), (^1S_1^{(8)})]g\rangle + g \rightarrow \psi_Q + g, \\ e^+e^- &\rightarrow Z^0 \rightarrow |(Q\bar{Q})[(^1S_0^{(8)})]g\rangle + g \rightarrow h_Q + g, \\ e^+e^- &\rightarrow Z^0 \rightarrow |(Q\bar{Q})[(^1S_1^{(8)})]g\rangle + g \rightarrow \chi_{QJ} + g, \end{aligned}$$

where Q indicates the heavy quark c or b , respectively. It is noted that the unlisted color-singlet channels via the virtual photon are forbidden by considerations on angular momentum conservation and Bose statistics, as formalized in the Landau-Pomeranchuk-Yang theorem [33]. In the present study, we will focus on the dominant color-octet channels listed above, and the less important ones such as those via the virtual photon and those via the component $|(Q\bar{Q})[({}^1{}^3P_J^{(8)})]g\rangle$ (both color and v^2 -suppressed with respect to the corresponding case of the color-singlet S -wave state) will not be discussed ¹.

Principally, there are two approaches to deal with the heavy meson hadroproduction. One is the fragmentation approach, which automatically sums up the dominant contributions, including some important higher order effects, into the total/differential cross sections by using the Dokshitzer-Gribov-Lipatov-Altarelli-Parisi evolution equation. The fragmentation approach is comparatively simple, one can easily accomplish a leading logarithm order or even higher order calculation. However the fragmentation approach is satisfied only in the cases when one is only interested in the produced meson itself, i.e. it treats the co-produced objects inclusively, thus losing any information about the co-produced objects. The other one is the so-called complete calculation approach, in which we directly deal with the full hard scattering amplitude without any approximations. In this approach it is sometimes hard to derive the analytical expression even at the leading order, but the information on the accompanying quark or gluon jets is retained and can be compared to data. In the present paper, we will mainly adopt the complete pQCD calculation approach to deal with these channels.

In comparison to the B factories as BaBar and Belle, we will show that a large number of heavy quarkonium events can be generated due to the Z^0 -boson resonance effect. Some features of heavy quarkonium production at such super Z factory has already been discussed in Refs.[34–40]. In this paper we focus on some novel observations. For example, when the quarkonium is produced directly in color-singlet state in the channel $e^+e^- \rightarrow Z^0 \rightarrow |H_{Q\bar{Q}}\rangle + Q\bar{Q}$, the spin-singlet and the spin-triplet S -wave states are almost equally probable (approximate “spin degeneracy”).

The remaining part of the paper is organized as follows. In Sec.II, we present the calculation technique for dealing with the heavy quarkonium production processes $e^+e^- \rightarrow |H_{Q\bar{Q}}\rangle + Q\bar{Q}$ and $e^+e^- \rightarrow |H_{Q\bar{Q}}\rangle + gg$, where the intermediate $(Q\bar{Q})$ -state is in either color-singlet or color-octet state respectively. In Sec.III, we present our numerical results. Total and differential cross sections are discussed, and an alternative proof of the above mentioned “spin degeneracy” is provided in the framework of the fragmentation approach. Sec.IV is reserved for a summary.

II. FORMULATION AND TECHNIQUE

According to the NRQCD framework, the differential cross section for the process, $e^+e^- \rightarrow |H_{Q\bar{Q}}\rangle + X$, can be factorized as [16, 41] :

$$d\sigma = \sum_n d\hat{\sigma}(e^+e^- \rightarrow (Q\bar{Q})[n] + X) \frac{\langle 0|\mathcal{O}^H(n)|0\rangle}{N_{col}N_{pol}}. \quad (5)$$

The production matrix element $\langle 0|\mathcal{O}^H(n)|0\rangle$ is proportional to the inclusive transition probability of the intermediate perturbative $(Q\bar{Q})$ -pair in $[n]$ -state into the final bound-state $|H_{Q\bar{Q}}\rangle$. The symbol $[n] = [m^{2S+1}L_J^{(1),(8)}]$ denotes the energy level m , the spin S , the orbital angular momentum L and the total angular momentum J of the intermediate $(Q\bar{Q})$ -pair, i.e.,

$$n = 1^1S_0, 2^1S_0, 1^1P_1, 1^1S_0^{(8)}; 1^3S_1, 2^3S_1, 1^3P_J, 1^3S_1^{(8)},$$

with $J = 0, 1, 2$. These states provide the dominant contributions to the processes $e^+e^- \rightarrow \gamma^*/Z^0 \rightarrow |H_{Q\bar{Q}}\rangle + Q\bar{Q}$ and $e^+e^- \rightarrow \gamma^*/Z^0 \rightarrow |H_{Q\bar{Q}}\rangle + gg$ up to $\mathcal{O}(v^4)$. The parameters N_{col} and N_{pol} refer to the number of colors and polarization states of the intermediate $(Q\bar{Q})$ -pair. $N_{col} = 1$ for the color-singlet state or $N_{col} = 8$ for the color-octet state. The color-singlet matrix elements can be directly related either to the wave function at the origin or (depending on the Fock state) to the first derivative of the wave function at the origin, which can be computed via potential models and/or potential NRQCD and/or lattice QCD. The color-octet matrix elements can be estimated by using the velocity scaling rule or be determined experimentally.

¹ There are other less important channels, either color suppressed or v suppressed or phase-space suppressed. We will not discuss them in the present paper either. For example, we have numerically obtained small total cross-sections for the channel $e^+e^- \rightarrow |H_{Q\bar{Q}}\rangle + gg$ with $H_{Q\bar{Q}}$ in the color-singlet P -wave states, in agreement with the v^2 -suppression with respect to the same channel with $H_{Q\bar{Q}}$ in the color-singlet S -wave states.

The short-distance cross section $d\hat{\sigma}(e^+(p_2)e^-(p_1) \rightarrow (Q\bar{Q})[n] + X)$ can be written in the following form:

$$d\hat{\sigma}(e^+e^- \rightarrow (Q\bar{Q})[n] + X) = \frac{\overline{\sum} |\mathcal{M}|^2 d\Phi_k}{4\sqrt{(p_1 \cdot p_2)^2 - m_e^4}}, \quad (6)$$

where k stands for the number of final state particles, $\overline{\sum}$ means that we need to average over the spin states of the initial particles and to sum over the spin and color of all final particles². The phase space with k final-state particles is

$$d\Phi_k = (2\pi)^4 \delta^4 \left(p_1 + p_2 - \sum_{f=3}^{k+2} p_f \right) \prod_{f=3}^{k+2} \frac{d^3 p_f}{(2\pi)^3 2p_f^0}.$$

The phase-space integration can be done with the help of a combination of the subroutines RAMBOS [42] and VEGAS [43], which can be found in the generators GENXICC [44] and BCVEGPY [45]. After generating proper phase-space points, one can calculate the numerical value for the squared amplitude $|\mathcal{M}|^2$. For the alternative calculations in the fragmentation approach, the phase space is calculated in a factorized form, as described in the appendix.

The hard scattering amplitude for those processes can be written as

$$i\mathcal{M} = \mathcal{C} L_{rr'}^\mu D_{\mu\nu} \sum_{j=1}^{j_{\max}} \mathcal{A}_j^\nu, \quad (7)$$

where the leptonic current

$$L_{rr'}^\mu = \bar{v}_r(p_2) \Gamma^\mu u_{r'}(p_1), \quad (8)$$

with the indices r and r' standing for the spin projections of the initial electron and positron. The value of j_{\max} is process dependent, e.g.

$$\begin{aligned} j_{\max} &= 4 \text{ for } e^+e^- \rightarrow (Q\bar{Q})[n] + Q\bar{Q}, \\ j_{\max} &= 6 \text{ for } e^+e^- \rightarrow (Q\bar{Q})[n] + gg, \end{aligned}$$

for $(Q\bar{Q})[n]$ in color-singlet state, while, for the case of color-octet production,

$$\begin{aligned} j_{\max} &= 2 \text{ for } e^+e^- \rightarrow Z^0 \rightarrow |(Q\bar{Q})[1^1 S_0^{(8)}]g\rangle + g, \\ j_{\max} &= 2 \text{ for } e^+e^- \rightarrow Z^0 \rightarrow |(Q\bar{Q})[1^3 S_1^{(8)}]g\rangle + g, \\ j_{\max} &= 6 \text{ for } e^+e^- \rightarrow Z^0 \rightarrow |(Q\bar{Q})[1^1 S_0^{(8)}]g\rangle + Q\bar{Q}, \\ j_{\max} &= 8 \text{ for } e^+e^- \rightarrow Z^0 \rightarrow |(Q\bar{Q})[1^3 S_1^{(8)}]g\rangle + Q\bar{Q}. \end{aligned}$$

For quarkonium production through the Z^0 -boson propagator, the vertex is $\Gamma^\mu = \gamma^\mu(1 - 4\sin^2\theta_w - \gamma^5)$ and the propagator is $D_{\mu\nu} = \frac{i}{k^2 - m_Z^2 + im_Z\Gamma_z} (-g_{\mu\nu} + k_\mu k_\nu / k^2)$, where Γ_z stands for the total decay width of the Z^0 boson. For quarkonium production through the virtual photon propagator, the vertex is $\Gamma^\mu = \gamma^\mu$ and the propagator is $D_{\mu\nu} = -\frac{i}{k^2} g_{\mu\nu}$.

The overall constant \mathcal{C} is different for the production via color-singlet (\mathcal{C}_s) and via color-octet $Q\bar{Q}$ state (\mathcal{C}_o). Expressions for the reduced hard scattering amplitudes \mathcal{A}_j^ν , which are process dependent, will be given in the following subsections.

² Because of the presence of (hereafter defined) projectors, the dimension of the short-distance cross section $\hat{\sigma}$ is [pb][GeV⁻³] for S -wave states and [pb][GeV⁻⁵] for P -wave states, which ensures the unit of the total cross section σ be the wanted [pb].

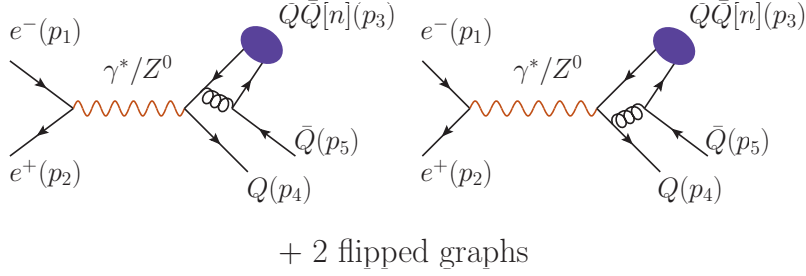


FIG. 1: Feynman diagrams for $e^+e^- \rightarrow |H_{Q\bar{Q}}\rangle + Q\bar{Q}$ via the perturbative state $(Q\bar{Q})[n]$. Here Q stands for c or b quark, and $[n]$ indicates the quantum numbers of the heavy quarkonium state.

A. Color-Singlet Case

$$1. \quad e^+(p_2)e^-(p_1) \rightarrow |H_{Q\bar{Q}}\rangle(p_3) + Q(p_4)\bar{Q}(p_5)$$

Typical Feynman diagrams for the process $e^+e^- \rightarrow |H_{Q\bar{Q}}\rangle + Q\bar{Q}$ through color-singlet $(Q\bar{Q})$ -quarkonium states are presented in Fig. 1. According to the Feynman diagrams, we can write down the reduced hard scattering amplitudes \mathcal{A}_j^ν of the short-distance cross-section $d\hat{\sigma}(e^+e^- \rightarrow (Q\bar{Q})[n] + Q\bar{Q})$.

For the color-singlet production of S -wave states, we have

$$\mathcal{A}_1^\nu = \bar{u}_s(p_4)\Gamma_{Q\bar{Q}}^\nu \frac{-\not{p}_3 - \not{p}_5 + m_Q}{(p_3 + p_5)^2 - m_Q^2} \gamma_\rho \frac{\Pi_{(Q\bar{Q})}^{0(1)}(p_3)}{(p_{31} + p_5)^2} \gamma^\rho v_{s'}(p_5), \quad (9)$$

$$\mathcal{A}_2^\nu = \bar{u}_s(p_4)\gamma_\rho \frac{\not{p}_4 + \not{p}_5 + \not{p}_{31} + m_Q}{(p_4 + p_5 + p_{31})^2 - m_Q^2} \Gamma_{Q\bar{Q}}^\nu \frac{\Pi_{(Q\bar{Q})}^{0(1)}(p_3)}{(p_{31} + p_5)^2} \gamma^\rho v_{s'}(p_5), \quad (10)$$

$$\mathcal{A}_3^\nu = \bar{u}_s(p_4)\gamma_\rho \frac{\Pi_{(Q\bar{Q})}^{0(1)}(p_3)}{(p_{32} + p_4)^2} \gamma^\rho \frac{\not{p}_3 + \not{p}_4 + m_Q}{(p_3 + p_4)^2 - m_Q^2} \Gamma_{Q\bar{Q}}^\nu v_{s'}(p_5), \quad (11)$$

$$\mathcal{A}_4^\nu = \bar{u}_s(p_4)\gamma_\rho \frac{\Pi_{(Q\bar{Q})}^{0(1)}(p_3)}{(p_{32} + p_4)^2} \Gamma_{Q\bar{Q}}^\nu \frac{-\not{p}_4 - \not{p}_5 - \not{p}_{32} + m_Q}{(p_4 + p_5 + p_{32})^2 - m_Q^2} \gamma^\rho v_{s'}(p_5). \quad (12)$$

For the color-singlet production of P -wave states, we have

$$\mathcal{A}_1^{\nu, S=0, L=1} = \bar{u}_s(p_4)\epsilon_\alpha^l(p_3) \frac{d}{dq_\alpha} \left[\Gamma_{Q\bar{Q}}^\nu \frac{-\not{p}_3 - \not{p}_5 + m_Q}{(p_3 + p_5)^2 - m_Q^2} \gamma_\rho \frac{\Pi_{(Q\bar{Q})}^0(p_3)}{(p_{31} + p_5)^2} \gamma^\rho \right]_{q=0} v_{s'}(p_5), \quad (13)$$

$$\mathcal{A}_2^{\nu, S=0, L=1} = \bar{u}_s(p_4)\epsilon_\alpha^l(p_3) \frac{d}{dq_\alpha} \left[\gamma_\rho \frac{\not{p}_4 + \not{p}_5 + \not{p}_{31} + m_Q}{(p_4 + p_5 + p_{31})^2 - m_Q^2} \Gamma_{Q\bar{Q}}^\nu \frac{\Pi_{(Q\bar{Q})}^0(p_3)}{(p_{31} + p_5)^2} \gamma^\rho \right]_{q=0} v_{s'}(p_5), \quad (14)$$

$$\mathcal{A}_3^{\nu, S=0, L=1} = \bar{u}_s(p_4)\epsilon_\alpha^l(p_3) \frac{d}{dq_\alpha} \left[\gamma_\rho \frac{\Pi_{(Q\bar{Q})}^0(p_3)}{(p_{32} + p_4)^2} \gamma^\rho \frac{\not{p}_3 + \not{p}_4 + m_Q}{(p_3 + p_4)^2 - m_Q^2} \Gamma_{Q\bar{Q}}^\nu \right]_{q=0} v_{s'}(p_5), \quad (15)$$

$$\mathcal{A}_4^{\nu, S=0, L=1} = \bar{u}_s(p_4)\epsilon_\alpha^l(p_3) \frac{d}{dq_\alpha} \left[\gamma_\rho \frac{\Pi_{(Q\bar{Q})}^0(p_3)}{(p_{32} + p_4)^2} \Gamma_{Q\bar{Q}}^\nu \frac{-\not{p}_4 - \not{p}_5 - \not{p}_{32} + m_Q}{(p_4 + p_5 + p_{32})^2 - m_Q^2} \gamma^\rho \right]_{q=0} v_{s'}(p_5) \quad (16)$$

and

$$\mathcal{A}_1^{\nu, S=1, L=1} = \bar{u}_s(p_4)\varepsilon_{\alpha\beta}^{J_z}(p_3) \frac{d}{dq_\alpha} \left[\Gamma_{Q\bar{Q}}^\nu \frac{-\not{p}_3 - \not{p}_5 + m_Q}{(p_3 + p_5)^2 - m_Q^2} \gamma_\rho \frac{\Pi_{(Q\bar{Q})}^\beta(p_3)}{(p_{31} + p_5)^2} \gamma^\rho \right]_{q=0} v_{s'}(p_5), \quad (17)$$

$$\mathcal{A}_2^{\nu, S=1, L=1} = \bar{u}_s(p_4)\varepsilon_{\alpha\beta}^{J_z}(p_3) \frac{d}{dq_\alpha} \left[\gamma_\rho \frac{\not{p}_4 + \not{p}_5 + \not{p}_{31} + m_Q}{(p_4 + p_5 + p_{31})^2 - m_Q^2} \Gamma_{Q\bar{Q}}^\nu \frac{\Pi_{(Q\bar{Q})}^\beta(p_3)}{(p_{31} + p_5)^2} \gamma^\rho \right]_{q=0} v_{s'}(p_5), \quad (18)$$

$$\mathcal{A}_3^{\nu, S=1, L=1} = \bar{u}_s(p_4) \varepsilon_{\alpha\beta}^{J_z}(p_3) \frac{d}{dq_\alpha} \left[\gamma_\rho \frac{\Pi_{(Q\bar{Q})}^\beta(p_3)}{(p_{32} + p_4)^2} \gamma^\rho \frac{\not{p}_3 + \not{p}_4 + m_Q}{(p_3 + p_4)^2 - m_Q^2} \Gamma_{Q\bar{Q}}^\nu \right]_{q=0} v_{s'}(p_5), \quad (19)$$

$$\mathcal{A}_4^{\nu, S=1, L=1} = \bar{u}_s(p_4) \varepsilon_{\alpha\beta}^{J_z}(p_3) \frac{d}{dq_\alpha} \left[\gamma_\rho \frac{\Pi_{(Q\bar{Q})}^\beta(p_3)}{(p_{32} + p_4)^2} \Gamma_{Q\bar{Q}}^\nu \frac{-\not{p}_4 - \not{p}_5 - \not{p}_{32} + m_Q}{(p_4 + p_5 + p_{32})^2 - m_Q^2} \gamma^\rho \right]_{q=0} v_{s'}(p_5). \quad (20)$$

Throughout the paper, we adopt the convention that the dummy index indicates summation. The parameters s and s' stand for the spin projections of the outgoing quark and antiquark respectively. The symbol s stands for the spin angular momentum quantum number, l stands for the radial angular momentum quantum number, $J_z = s_z + l_z$ stands for the z -component of the total angular momentum quantum number of the bound state, respectively.

For convenience, we have introduced a general interaction vertex

$$\Gamma_{Q\bar{Q}}^\nu = \gamma^\nu (\xi_1 P_L + \xi_2 P_R), \quad (21)$$

where $P_L = (1 - \gamma^5)/2$ and $P_R = (1 + \gamma^5)/2$. Here $\xi_1 = 2 - \frac{8}{3} \sin^2 \theta_w$ and $\xi_2 = -\frac{8}{3} \sin^2 \theta_w$ for $(Zc\bar{c})$ -vertex, $\xi_1 = 2 - \frac{4}{3} \sin^2 \theta_w$ and $\xi_2 = -\frac{4}{3} \sin^2 \theta_w$ for $(Zb\bar{b})$ -vertex, $\xi_1 = 1$ and $\xi_2 = 1$ for $(\gamma^* Q\bar{Q})$ -vertex, respectively.

The momenta of the constituent quarks are

$$p_{31} = \frac{m_Q}{M_{Q\bar{Q}}} p_3 + q \quad \text{and} \quad p_{32} = \frac{m_{\bar{Q}}}{M_{Q\bar{Q}}} p_3 - q, \quad (22)$$

where $M_{Q\bar{Q}} = m_Q + m_{\bar{Q}}$ is implicitly adopted to ensure the gauge invariance of the hard scattering amplitude, q is the relative momentum between the two constituent quarks inside the quarkonium.

The covariant forms of the projectors are

$$\Pi_{(Q\bar{Q})}^0(p_3) = \frac{-\sqrt{M_{Q\bar{Q}}}}{4m_Q m_{\bar{Q}}} (\not{p}_{32} - m_{\bar{Q}}) \gamma_5 (\not{p}_{31} + m_Q) \quad (23)$$

and

$$\Pi_{(Q\bar{Q})}^1(p_3) = \epsilon_\kappa^s(p_3) \Pi_{(Q\bar{Q})}^\kappa(p_3), \quad (24)$$

where $\epsilon^s(p_3)$ stands for the polarization vector of the spin-triplet S -wave state and

$$\Pi_{(Q\bar{Q})}^\kappa(p_3) = \frac{-\sqrt{M_{Q\bar{Q}}}}{4m_Q m_{\bar{Q}}} (\not{p}_{32} - m_{\bar{Q}}) \gamma^\kappa (\not{p}_{31} + m_Q). \quad (25)$$

Inserting these projectors into the amplitude, the amplitude can be squared, summed over the spin in the final state and averaged over the ones in the initial state. The selection of the proper angular momentum is done by performing a suitable polarization sum. For examples, the sum over polarization for a spin-triplet S -wave state (3S_1) or a spin-singlet P -wave state (1P_1) is given by:

$$\sum_{J_z} \epsilon_\alpha(p_3) \epsilon_{\alpha'}^*(p_3) = \Pi_{\alpha\alpha'}, \quad (26)$$

where $\epsilon(p_3)$ stands for the polarization vector of the meson, $\epsilon(p_3) = \epsilon^s(p_3)$ and $J_z = s_z$ for the 3S_1 state, $\epsilon(p_3) = \epsilon^l(p_3)$ and $J_z = l_z$ for the spin-singlet 1P_1 state. And the sum over polarization for the spin-triplet P -wave states (3P_J with $J = 0, 1, 2$) is given by [41]

$$\begin{aligned} \varepsilon_{\alpha\beta}^{(0)}(p_3) \varepsilon_{\alpha'\beta'}^{(0)*}(p_3) &= \frac{1}{3} \Pi_{\alpha\beta} \Pi_{\alpha'\beta'} \\ \sum_{J_z} \varepsilon_{\alpha\beta}^{(1)}(p_3) \varepsilon_{\alpha'\beta'}^{(1)*}(p_3) &= \frac{1}{2} [\Pi_{\alpha\alpha'} \Pi_{\beta\beta'} - \Pi_{\alpha\beta'} \Pi_{\alpha'\beta}] \\ \sum_{J_z} \varepsilon_{\alpha\beta}^{(2)}(p_3) \varepsilon_{\alpha'\beta'}^{(2)*}(p_3) &= \frac{1}{2} [\Pi_{\alpha\alpha'} \Pi_{\beta\beta'} + \Pi_{\alpha\beta'} \Pi_{\alpha'\beta}] - \frac{1}{3} \Pi_{\alpha\beta} \Pi_{\alpha'\beta'}, \end{aligned}$$

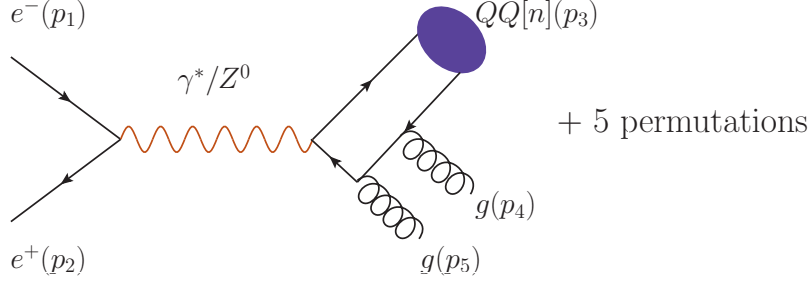


FIG. 2: Typical Feynman diagrams for $e^+e^- \rightarrow |H_{Q\bar{Q}}\rangle + gg$ through the perturbative state $(Q\bar{Q})[n]$. Here Q stands for the c or b quark, and $[n]$ indicates the quantum numbers of the heavy quarkonium state.

where $\varepsilon_{\alpha\beta}^{(J)}(p_3)$ stands for the polarization tensor of the spin-triplet P -wave states. In the above formulas, we have defined a short notation for the polarization sum, i.e.

$$\Pi_{\rho_1\rho_2} \equiv -g_{\rho_1\rho_2} + \frac{p_{3\rho_1}p_{3\rho_2}}{M_{Q\bar{Q}}^2}, \quad (27)$$

where ρ_1 and ρ_2 , which equal to $0, \dots, 4$ respectively, are Lorentz indices of the meson momentum p_3 .

For the overall color-singlet parameter (\mathcal{C} in Eq.(7)), we have $\mathcal{C}_s = \frac{4}{3\sqrt{3}} \frac{e^2 g_s^2}{\sin^2 \theta_w \cdot (4 \cos \theta_w)^2} \delta_{ij}$ for the quarkonium production through Z^0 -boson propagator and $\mathcal{C}_s = \frac{4}{3\sqrt{3}} e_Q e^2 g_s^2 \delta_{ij}$ for the quarkonium production through virtual photon propagator, where e_Q stands for the electric charge of Q in unit e . The symbols $i, j = (1, 2, 3)$ in δ_{ij} are color-indices for the outgoing antiquark and quark, respectively. Here g_s stands for the gauge coupling of QCD, which is connected with the strong coupling α_s via the relation $\alpha_s = g_s^2/4\pi$, and θ_w is the weak mixing angle.

$$2. \quad e^+(p_2)e^-(p_1) \rightarrow |H_{Q\bar{Q}}\rangle(p_3) + g(p_4)g(p_5)$$

Typical Feynman diagrams for the process $e^+e^- \rightarrow |H_{Q\bar{Q}}\rangle + gg$ are presented in Fig. 2. According to the Feynman diagrams, one can write down the reduced hard scattering amplitudes \mathcal{A}_j^ν for the short-distance cross-section $d\hat{\sigma}(e^+e^- \rightarrow (Q\bar{Q})[n] + gg)$ as

$$\mathcal{A}_1^\nu = \text{Tr} \left[\left(\Pi_{(Q\bar{Q})}^{0(1)}(p_3) \right) \Gamma_{Q\bar{Q}}^\nu \frac{-\not{p}_{32} - \not{p}_4 - \not{p}_5 + m_Q}{(p_{32} + p_4 + p_5)^2 - m_Q^2} \not{\epsilon}(p_5) \frac{-\not{p}_{32} - \not{p}_4 + m_Q}{(p_{32} + p_4)^2 - m_Q^2} \not{\epsilon}(p_4) \right], \quad (28)$$

and the amplitudes $\mathcal{A}_2^\nu, \dots, \mathcal{A}_6^\nu$ can be derived by permutations.

For the overall color-singlet parameter, we have $\mathcal{C}_s = \frac{1}{2\sqrt{3}} \frac{e^2 g_s^2}{\sin^2 \theta_w \cdot (4 \cos \theta_w)^2} \delta_{ab}$ for the quarkonium production through Z^0 -boson propagator and $\mathcal{C}_s = \frac{1}{2\sqrt{3}} e_Q e^2 g_s^2 \delta_{ab}$ for the quarkonium production through virtual photon propagator, where $a, b = (1, \dots, 8)$ are color indices of the two outgoing gluons.

The reduced amplitudes for the case of color-singlet P -wave states can be written down in a similar way as for the process $e^+e^- \rightarrow |H_{Q\bar{Q}}\rangle + Q\bar{Q}$. Numerically, it is found that the total cross-sections for the color-singlet P -wave states are negligible, so we do not present their reduced amplitudes here.

B. Color-Octet Case

$$1. \quad e^+(p_2)e^-(p_1) \rightarrow Z^0 \rightarrow |(Q\bar{Q})[(1^1 S_0^{(8)})], (1^3 S_1^{(8)})]g\rangle(p_3) + Q(p_4)\bar{Q}(p_5)$$

Typical Feynman diagrams for the processes $e^+e^- \rightarrow Z^0 \rightarrow |(Q\bar{Q})[(1^1 S_0^{(8)})]g\rangle + Q\bar{Q}$ and $e^+e^- \rightarrow Z^0 \rightarrow |(Q\bar{Q})[(1^3 S_1^{(8)})]g\rangle + Q\bar{Q}$ are presented in Figs. 3 and 4, respectively. It is found that

- The four Feynman diagrams shown in Fig. 3a and Fig. 4a have the same topologies as those of Fig. 1. Their reduced amplitudes $\mathcal{A}'_1, \dots, \mathcal{A}'_4$ are the same as those of Eqs.(9,10,11,12), with the overall parameter \mathcal{C}_s replaced by \mathcal{C}_o , and the color-singlet matrix element replaced by the color-octet one.
- The two Feynman diagrams shown in Fig. 3b and Fig. 4b have the same topologies, and their reduced amplitudes \mathcal{A}'_5 and \mathcal{A}'_6 are the same:

$$\mathcal{A}'_5 = \bar{u}_s(p_4)\gamma_\rho \text{Tr} \left[\gamma^\rho \frac{\Pi_{(Q\bar{Q})}^{0(1)}(p_3)}{(p_4 + p_5)^2} \Gamma_{Q\bar{Q}}^\nu \frac{-\not{p}_{32} - \not{p}_4 - \not{p}_5 + m_Q}{(p_{32} + p_4 + p_5)^2 - m_Q^2} \right] v_{s'}(p_5), \quad (29)$$

$$\mathcal{A}'_6 = \bar{u}_s(p_4)\gamma_\rho \text{Tr} \left[\gamma^\rho \frac{\not{p}_{31} + \not{p}_4 + \not{p}_5 + m_Q}{(p_{31} + p_4 + p_5)^2 - m_Q^2} \Gamma_{Q\bar{Q}}^\nu \frac{\Pi_{(Q\bar{Q})}^{0(1)}(p_3)}{(p_4 + p_5)^2} \right] v_{s'}(p_5). \quad (30)$$

- The remaining two reduced amplitudes \mathcal{A}'_7 and \mathcal{A}'_8 for the case of $|(Q\bar{Q})[1^3S_0^{(8)}]\rangle|g\rangle$ production, as shown in Fig. 4c, are

$$\mathcal{A}'_7 = \bar{u}_s(p_4)\Gamma_{Q\bar{Q}}^\nu \frac{-\not{p}_3 - \not{p}_5 + m_Q}{(p_3 + p_5)^2 - m_Q^2} \gamma_\rho \text{Tr} \left[\frac{\Pi_{(Q\bar{Q})}^1(p_3)}{p_3^2} \gamma^\rho \right] v_{s'}(p_5), \quad (31)$$

$$\mathcal{A}'_8 = \bar{u}_s(p_4)\gamma_\rho \text{Tr} \left[\frac{\Pi_{(Q\bar{Q})}^1(p_3)}{p_3^2} \gamma^\rho \right] \frac{\not{p}_3 + \not{p}_4 + m_Q}{(p_3 + p_4)^2 - m_Q^2} \Gamma_{Q\bar{Q}}^\nu v_{s'}(p_5). \quad (32)$$

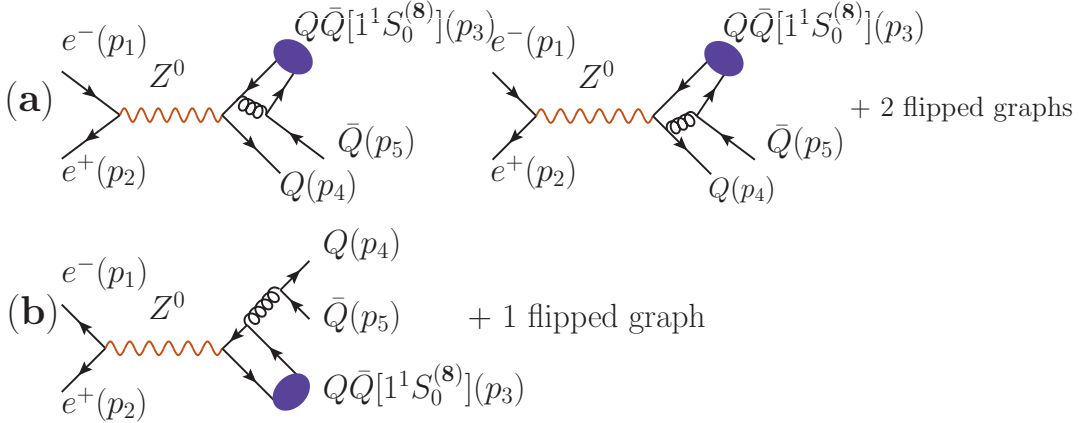


FIG. 3: Typical Feynman diagrams for $e^+e^- \rightarrow Z^0 \rightarrow |(Q\bar{Q})[1^1S_0^{(8)}]\rangle|g\rangle + Q\bar{Q}$, where Q stands for c or b quark.

For the overall color-octet parameters, we have $\mathcal{C}_o = \frac{e^2 g_s^2}{\sin^2 \theta_w (4 \cos \theta_w)^2} \times (\mathcal{C}_{ij}^{(a)}, \mathcal{C}_{ij}^{(b)}, \mathcal{C}_{ij}^{(c)})$ respectively. Here, the color factors $\mathcal{C}_{ij}^{(a),(b),(c)}$, according to Figs. 4a, 4b and 4c, are:

$$\mathcal{C}_{ij}^{(a)} = \sum_{m,n} (T^a)_{in} \times (\sqrt{2}T^d)_{nm} \times (T^a)_{mj}, \quad (33)$$

$$\mathcal{C}_{ij}^{(b)} = \sum_{m,n} (T^a)_{ij} \times (T^a)_{mn} \times (\sqrt{2}T^d)_{nm}, \quad (34)$$

$$\mathcal{C}_{ij}^{(c)} = \sum_{m,n} (T^a)_{ij} \times (T^a)_{mn} \times (\sqrt{2}T^d)_{nm}, \quad (35)$$

where $i, j = (1, 2, 3)$ are the color indices of the outgoing anti-quark \bar{Q} and quark Q , and $m, n = (1, 2, 3)$ are those of the two constituent quarks Q and \bar{Q} in the heavy quarkonium. The superscript indices $(a), (b)$ and (c) of \mathcal{C}_{ij} refer to

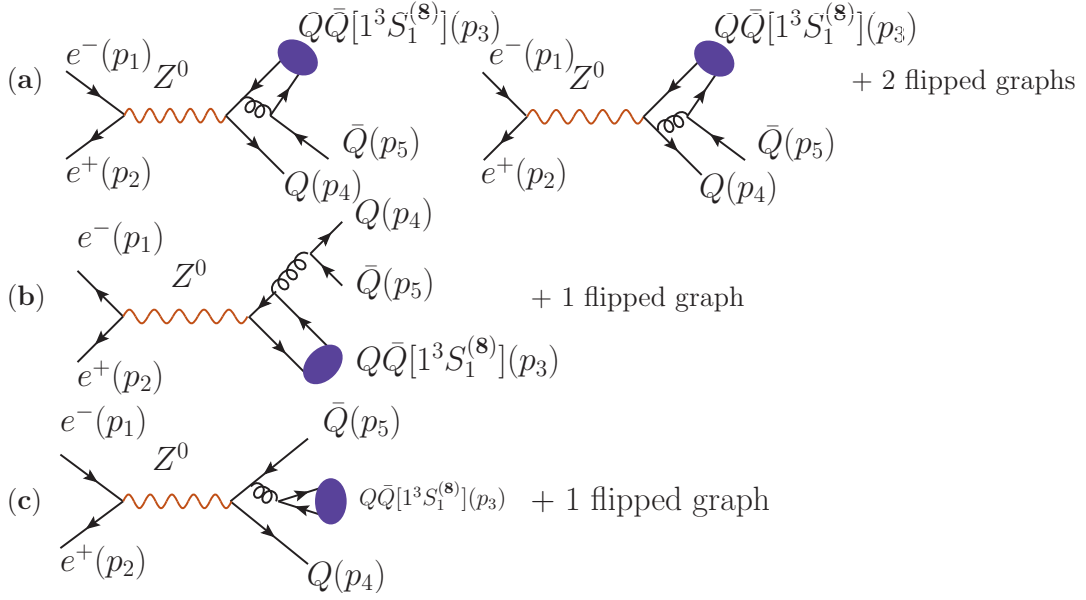


FIG. 4: Typical Feynman diagrams for $e^+e^- \rightarrow Z^0 \rightarrow |(Q\bar{Q})[(1^3S_1^{(8)})]g + Q\bar{Q}$, where Q stands for c or b quark.

the corresponding figures in Figs. 3 and 4. After simplification, we obtain

$$C_{ij}^{(a)} = -\frac{\sqrt{2}}{6}T_{ij}^d, \quad C_{ij}^{(b)} = C_{ij}^{(c)} = \frac{\sqrt{2}}{2}T_{ij}^d.$$

Here $d = (1, \dots, 8)$ represents the color of the color-octet quarkonium.

$$2. \quad e^+(p_2)e^-(p_1) \rightarrow Z^0 \rightarrow |(Q\bar{Q})[(1^1S_0^{(8)}), (1^3S_1^{(8)})]g + g(p_4)$$

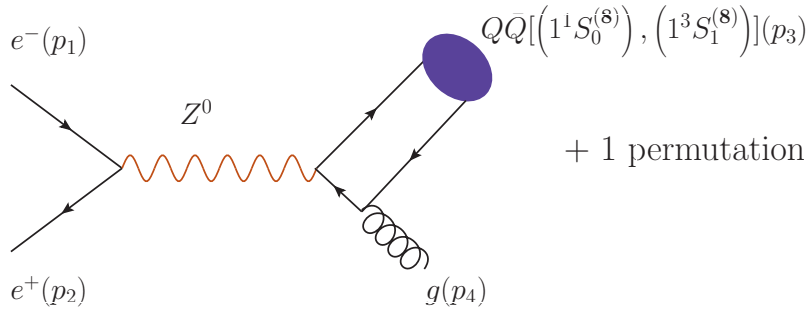


FIG. 5: Typical Feynman diagrams for $e^+e^- \rightarrow Z^0 \rightarrow |(Q\bar{Q})[(1^1S_0^{(8)}), (1^3S_1^{(8)})]g + g$, where Q stands for the heavy c or b quark.

Typical Feynman diagrams for the processes $e^+e^- \rightarrow Z^0 \rightarrow |(Q\bar{Q})[(1^1S_0^{(8)}), (1^3S_1^{(8)})]g + g$ are presented in Fig. 5. The reduced amplitude \mathcal{A}_1^ν takes the form

$$\mathcal{A}_1^\nu = \text{Tr} \left[\left(\Pi_{(Q\bar{Q})}^{0(1)}(p_3) \right) \Gamma_{Q\bar{Q}}^\nu \frac{-\not{p}_{32} - \not{p}_4 + m_Q}{(p_{32} + p_4)^2 - m_Q^2} \not{\epsilon}(p_4) \right], \quad (36)$$

and \mathcal{A}_2^ν can be obtained from \mathcal{A}_1^ν by permutation.

For the overall color-octet parameter, we have $\mathcal{C}_o = \frac{\sqrt{2}}{2} \frac{e^2 g_s}{\sin^2 \theta_w (4 \cos \theta_w)^2} \times \delta_{ad}$. Here $a, d = (1, \dots, 8)$ represent the color indices of the outgoing gluon and of the color-octet quarkonium, respectively.

III. NUMERICAL RESULTS

Matrix elements	values [46]
$\langle 0 \mathcal{O}_1^{J/\psi}(^3S_1) 0\rangle$	1.2 GeV ³
$\langle 0 \mathcal{O}_1^{\psi'}(^3S_1) 0\rangle$	7.6×10^{-1} GeV ³
$\langle 0 \mathcal{O}_1^{\Upsilon}(^3S_1) 0\rangle$	9.3 GeV ³
$\langle 0 \mathcal{O}_1^{\Upsilon'}(^3S_1) 0\rangle$	4.6 GeV ³
$\langle 0 \mathcal{O}_1^{X_{c1}}(^3P_1) 0\rangle$	3.2×10^{-1} GeV ⁵
$\langle 0 \mathcal{O}_1^{X_{b1}}(^3P_1) 0\rangle$	6.1 GeV ⁵
$\langle 0 \mathcal{O}_8^{J/\psi}(^3S_1) 0\rangle$	1.2×10^{-2} GeV ³
$\langle 0 \mathcal{O}_8^{\Upsilon}(^3S_1) 0\rangle$	9.5×10^{-3} GeV ³
$\langle 0 \mathcal{O}_8^{X_{c1}}(^3S_1) 0\rangle$	1.6×10^{-2} GeV ³
$\langle 0 \mathcal{O}_8^{X_{b1}}(^3S_1) 0\rangle$	4.3×10^{-2} GeV ³

TABLE I: Input color-singlet and color-octet matrix elements.

In doing numerical calculation, the heavy quark masses are taken as: $m_c = 1.50_{-0.15}^{+0.15}$ GeV and $m_b = 4.90_{-0.15}^{+0.15}$ GeV. The color-singlet and color-octet non-perturbative matrix elements, taken from Ref.[46], are listed in Table I. The 1S_0 matrix elements, not listed in the table, are derived adopting the relation

$$\langle 0|\mathcal{O}_{[1,8]}^H(^3S_1)|0\rangle \simeq 3\langle 0|\mathcal{O}_{[1,8]}^H(^1S_0)|0\rangle.$$

The color-singlet matrix elements have been calculated using their relation to the wave functions at the origin [16, 41]:

$$\frac{\langle 0|\mathcal{O}_1^{\eta_c}|0\rangle}{2N_c} \simeq \frac{\langle 0|\mathcal{O}_1^{J/\psi}|0\rangle}{6N_c} = |\Psi_{1S}(0)|^2, \quad (37)$$

$$\frac{\langle 0|\mathcal{O}_1^{\eta_c'}|0\rangle}{2N_c} \simeq \frac{\langle 0|\mathcal{O}_1^{\psi'}|0\rangle}{6N_c} = |\Psi_{2S}(0)|^2 \quad (38)$$

and

$$\frac{\langle 0|\mathcal{O}_1^{X_{c0}}|0\rangle}{2N_c} \simeq \frac{\langle 0|\mathcal{O}_1^{X_{c1}}|0\rangle}{6N_c} \simeq \frac{\langle 0|\mathcal{O}_1^{X_{c2}}|0\rangle}{10N_c} = |\Psi'_{1P}(0)|^2. \quad (39)$$

For the production color-octet matrix elements, we adopt the relation [16]

$$\begin{aligned} \langle 0|\mathcal{O}_8^{X_{c2}}(^3S_1)|0\rangle &= \frac{5}{3}\langle 0|\mathcal{O}_8^{h_c}(^1S_0)|0\rangle, \\ \langle 0|\mathcal{O}_8^{X_{c1}}(^3S_1)|0\rangle &= \frac{3}{3}\langle 0|\mathcal{O}_8^{h_c}(^1S_0)|0\rangle, \\ \langle 0|\mathcal{O}_8^{X_{c0}}(^3S_1)|0\rangle &= \frac{1}{3}\langle 0|\mathcal{O}_8^{h_c}(^1S_0)|0\rangle. \end{aligned} \quad (40)$$

Here the heavy-quark spin symmetry [16] has been implicitly adopted. That is, we will not distinguish the wave-functions at the origin for the spin-singlet (1S_0) state and the spin-triplet (3S_1) state at the same energy level. The bottomonium color-singlet and color-octet matrix elements satisfy analogous relations [46].

As for the renormalization scale, we take it to be $2m_c$ for charmonium production, and $2m_b$ for bottomonium production. Other input parameters are taken from the Particle Data Group [47]: $\Gamma_Z = 2.4952$ GeV, $m_Z = 91.1876$ GeV, $\sin^2\theta_w = 0.2312$. By using the leading-order α_s running and $\alpha_s(m_Z) = 0.1184$, we obtain $\alpha_s(2m_c) = 0.237$ and $\alpha_s(2m_b) = 0.175$.

A. Properties of the color-singlet processes

The color-singlet components provide the dominant contributions to the heavy quarkonium production processes. We will make a detailed discussion on the properties of the color-singlet processes, including their total and differential cross sections and the uncertainties related to a variation of the e^+e^- collision energy with respect to the Z^0 -boson mass and to the knowledge of the heavy quark masses.

1. Total and differential cross sections

production channels	Total cross sections	
	Z^0 -propagator	γ^* -propagator
$e^+e^- \rightarrow \eta_c(1S) + c\bar{c}$	1.76	4.09×10^{-3}
$e^+e^- \rightarrow \eta'_c(2S) + c\bar{c}$	1.11	2.59×10^{-3}
$e^+e^- \rightarrow J/\psi(1S) + c\bar{c}$	1.83	4.39×10^{-3}
$e^+e^- \rightarrow \psi'(2S) + c\bar{c}$	1.16	2.78×10^{-3}
$e^+e^- \rightarrow J/\psi(1S) + gg$	3.84×10^{-2}	6.99×10^{-4}
$e^+e^- \rightarrow \psi'(2S) + gg$	2.43×10^{-2}	4.42×10^{-4}
$e^+e^- \rightarrow \eta_c(1S) + gg$	1.72×10^{-1}	0
$e^+e^- \rightarrow \eta'_c(2S) + gg$	1.09×10^{-1}	0
$e^+e^- \rightarrow h_c(1P) + c\bar{c}$	2.34×10^{-1}	5.60×10^{-4}
$e^+e^- \rightarrow \chi_{c0}(1P) + c\bar{c}$	3.32×10^{-1}	7.78×10^{-4}
$e^+e^- \rightarrow \chi_{c1}(1P) + c\bar{c}$	3.66×10^{-1}	8.37×10^{-4}
$e^+e^- \rightarrow \chi_{c2}(1P) + c\bar{c}$	1.44×10^{-1}	3.24×10^{-4}

TABLE II: Total cross section (in pb) for the color-singlet charmonium production. The channels are through Z^0 and γ^* propagators, respectively, for $\sqrt{s} = m_Z$ and $m_c = 1.5$ GeV.

production channels	Total cross sections	
	Z^0 -propagator	γ^* -propagator
$e^+e^- \rightarrow \eta_b(1S) + b\bar{b}$	1.94×10^{-1}	8.69×10^{-5}
$e^+e^- \rightarrow \eta'_b(2S) + b\bar{b}$	9.60×10^{-2}	4.30×10^{-5}
$e^+e^- \rightarrow \Upsilon(1S) + b\bar{b}$	2.18×10^{-1}	1.16×10^{-4}
$e^+e^- \rightarrow \Upsilon'(2S) + b\bar{b}$	1.08×10^{-1}	5.74×10^{-5}
$e^+e^- \rightarrow \Upsilon(1S) + gg$	6.54×10^{-2}	9.16×10^{-5}
$e^+e^- \rightarrow \Upsilon'(2S) + gg$	3.24×10^{-2}	4.53×10^{-5}
$e^+e^- \rightarrow \eta_b(1S) + gg$	8.18×10^{-2}	0
$e^+e^- \rightarrow \eta'_b(2S) + gg$	4.05×10^{-2}	0
$e^+e^- \rightarrow h_b(1P) + b\bar{b}$	6.84×10^{-3}	3.36×10^{-6}
$e^+e^- \rightarrow \chi_{b0}(1P) + b\bar{b}$	1.09×10^{-2}	5.18×10^{-6}
$e^+e^- \rightarrow \chi_{b1}(1P) + b\bar{b}$	1.04×10^{-2}	4.22×10^{-6}
$e^+e^- \rightarrow \chi_{b2}(1P) + b\bar{b}$	4.30×10^{-3}	1.67×10^{-6}

TABLE III: Total cross section (in pb) for the color-singlet bottomonium production. The channels are through Z^0 and γ^* propagators, respectively, for $\sqrt{s} = m_Z$ and $m_b = 4.9$ GeV.

Total cross sections for the charmonium and bottomonium productions at the Z^0 peak ($\sqrt{s} = m_Z$) are presented in Tables II and III. By adding all the $1S$ -wave charmonium or bottomonium states together, we obtain

$$\sigma(e^+e^- \rightarrow |H_{c\bar{c}}\rangle(1S) + c\bar{c}) \simeq 3.59 \text{ pb}$$

and

$$\sigma(e^+e^- \rightarrow |H_{b\bar{b}}\rangle(1S) + b\bar{b}) \simeq 0.41 \text{ pb.}$$

By adding all the $1P$ -wave charmonium or bottomonium states together, we obtain

$$\sigma(e^+e^- \rightarrow |H_{c\bar{c}}\rangle(1P) + c\bar{c}) \simeq 1.08 \text{ pb}$$

and

$$\sigma(e^+e^- \rightarrow |H_{b\bar{b}}\rangle(1P) + b\bar{b}) \simeq 3.25 \times 10^{-2} \text{ pb.}$$

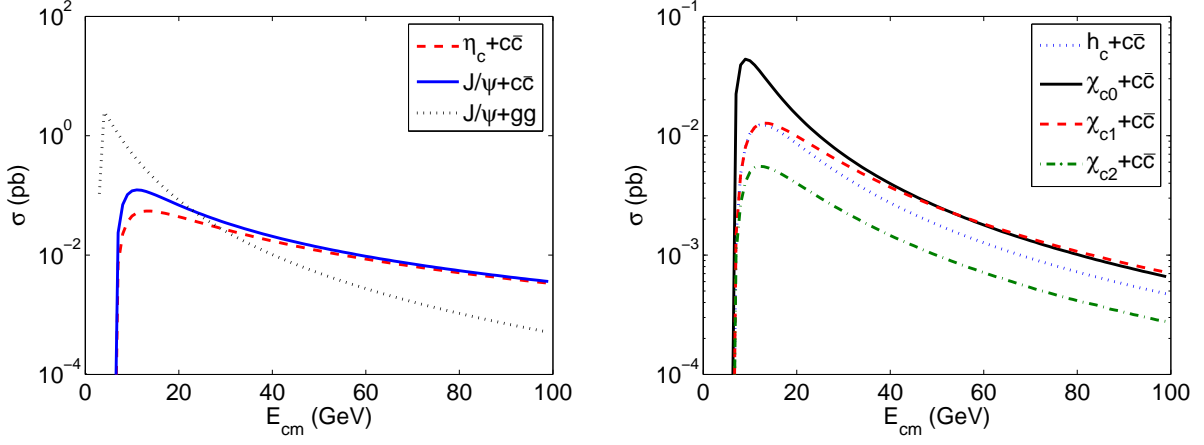


FIG. 6: Total cross sections of the channels $e^+ + e^- \rightarrow \gamma^* \rightarrow |H_{c\bar{c}}\rangle + X$ for different S wave and P wave charmonium states versus the e^+e^- collision energy $E_{cm} = \sqrt{s}$.

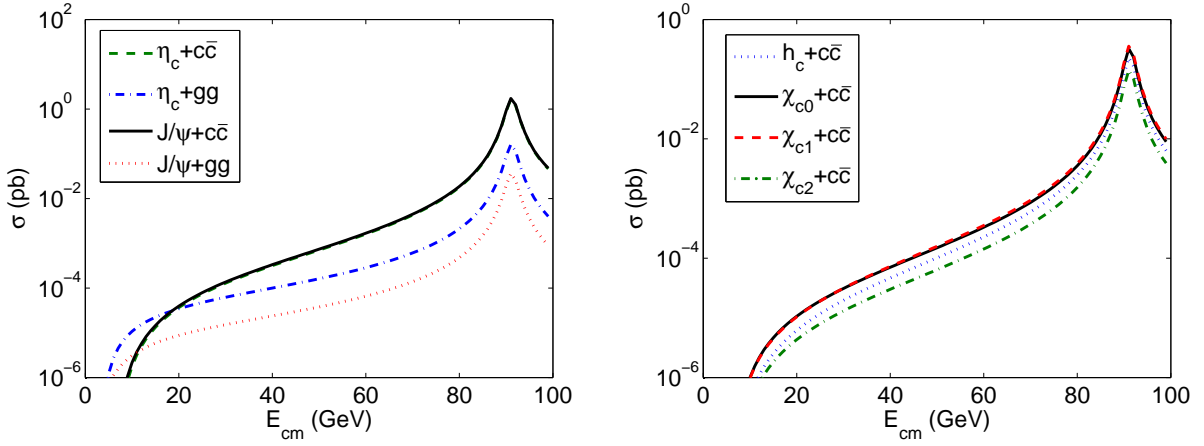


FIG. 7: Total cross sections of the channels $e^+ + e^- \rightarrow Z^0 \rightarrow |H_{c\bar{c}}\rangle + X$ for different S wave and P wave charmonium states versus the e^+e^- collision energy $E_{cm} = \sqrt{s}$. The two curves for $\eta_c + c\bar{c}$ and $J/\psi + c\bar{c}$ almost coincide with each other, and the two curves for $\chi_{c0} + c\bar{c}$ and $\chi_{c1} + c\bar{c}$ also almost coincide with each other.

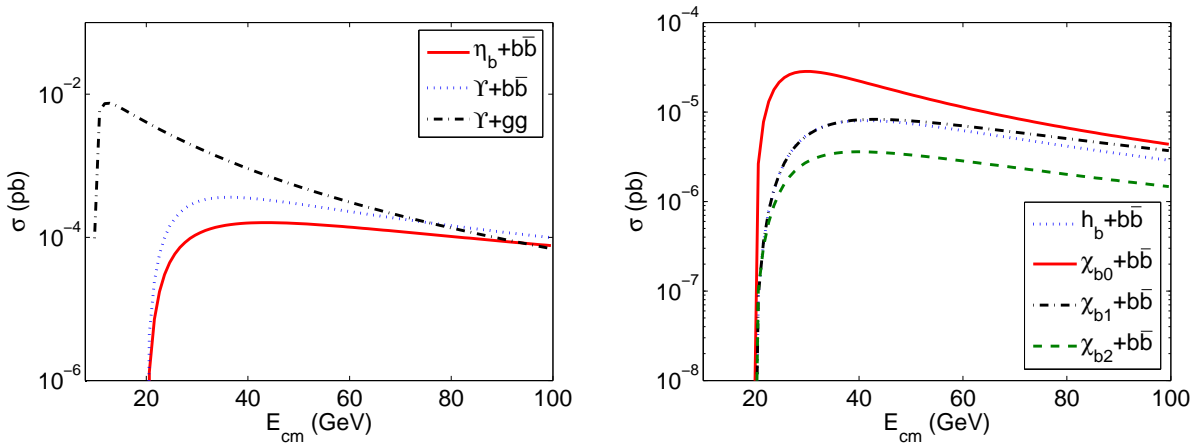


FIG. 8: Total cross sections of the channels $e^+ + e^- \rightarrow \gamma^* \rightarrow |H_{b\bar{b}}\rangle + X$ for different S wave and P wave bottomonium states versus the e^+e^- collision energy $E_{cm} = \sqrt{s}$.

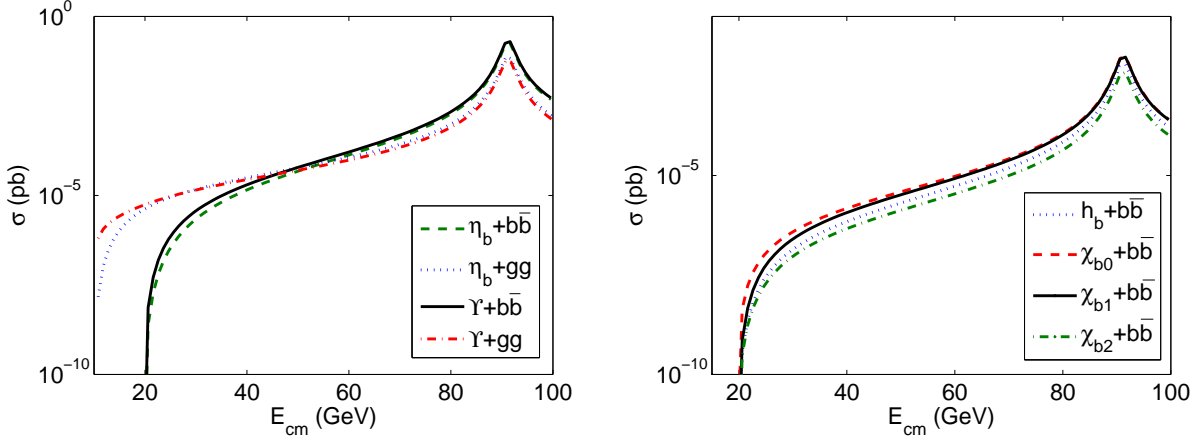


FIG. 9: Total cross sections of the channels $e^+e^- \rightarrow Z^0 \rightarrow |H_{bb}\rangle + X$ for different S wave and P wave bottomonium states versus the e^+e^- collision energy $E_{cm} = \sqrt{s}$. The two curves for $\eta_b + b\bar{b}$ and $\Upsilon + b\bar{b}$ almost coincide with each other, and the two curves for $\chi_{b0} + b\bar{b}$ and $\chi_{b1} + b\bar{b}$ also almost coincide with each other.

By adding all the $2S$ -wave charmonium or bottomonium states together, we obtain

$$\sigma(e^+e^- \rightarrow |H_{c\bar{c}}\rangle(2S) + c\bar{c}) \simeq 2.27 \text{ pb}$$

and

$$\sigma(e^+e^- \rightarrow |H_{b\bar{b}}\rangle(2S) + b\bar{b}) \simeq 0.20 \text{ pb}.$$

Then, in addition to the $1S$ -level quarkonium states, both the $2S$ -level and $1P$ -level quarkonium states can provide sizable contributions to the production channel $e^+e^- \rightarrow |H_{Q\bar{Q}}\rangle + Q\bar{Q}$. More explicitly, to show the relative importance of those channels via the Z^0 propagator, we define two type of ratios

$$R_{H_{c\bar{c}}+X} = \frac{\sigma_{e^+e^- \rightarrow Z^0 \rightarrow |H_{c\bar{c}}\rangle + X}}{\sigma_{e^+e^- \rightarrow Z^0 \rightarrow J/\psi + c\bar{c}}} \quad (41)$$

and

$$R_{H_{b\bar{b}}+X} = \frac{\sigma_{e^+e^- \rightarrow Z^0 \rightarrow |H_{b\bar{b}}\rangle + X}}{\sigma_{e^+e^- \rightarrow Z^0 \rightarrow \Upsilon + b\bar{b}}}. \quad (42)$$

We obtain

$$\begin{aligned} R_{\eta_c + gg} &= 9.4\%, \quad R_{\eta'_c + gg} = 6.0\%, \quad R_{J/\psi + gg} = 2.1\%, \\ R_{\psi' + gg} &= 1.3\%, \quad R_{\eta_c + c\bar{c}} = 96\%, \quad R_{\eta'_c + c\bar{c}} = 61\%, \\ R_{\psi' + c\bar{c}} &= 63\%, \quad R_{h_c + c\bar{c}} = 13\%, \quad R_{\chi_{c0} + c\bar{c}} = 18\%, \\ R_{\chi_{c1} + c\bar{c}} &= 20\%, \quad R_{\chi_{c2} + c\bar{c}} = 7.8\% \end{aligned}$$

and

$$\begin{aligned} R_{\eta_b + gg} &= 38\%, \quad R_{\eta'_b + gg} = 19\%, \quad R_{\Upsilon + gg} = 30\%, \\ R_{\Upsilon' + gg} &= 15\%, \quad R_{\eta_b + b\bar{b}} = 89\%, \quad R_{\eta'_b + b\bar{b}} = 44\%, \\ R_{\Upsilon' + b\bar{b}} &= 50\%, \quad R_{h_b + b\bar{b}} = 3.1\%, \quad R_{\chi_{b0} + b\bar{b}} = 5.0\%, \\ R_{\chi_{b1} + b\bar{b}} &= 4.8\%, \quad R_{\chi_{b2} + b\bar{b}} = 2.0\%. \end{aligned}$$

For the e^+e^- collision energy $E_{cm} = \sqrt{s} = m_Z$, the cross sections for the channels via the γ^* propagator are much smaller than the same channels via the Z^0 propagator. For example, we have

$$\frac{\sigma_{e^+e^- \rightarrow \gamma^* \rightarrow J/\psi + c\bar{c}}}{\sigma_{e^+e^- \rightarrow Z^0 \rightarrow J/\psi + c\bar{c}}} = 2.4 \times 10^{-3}$$

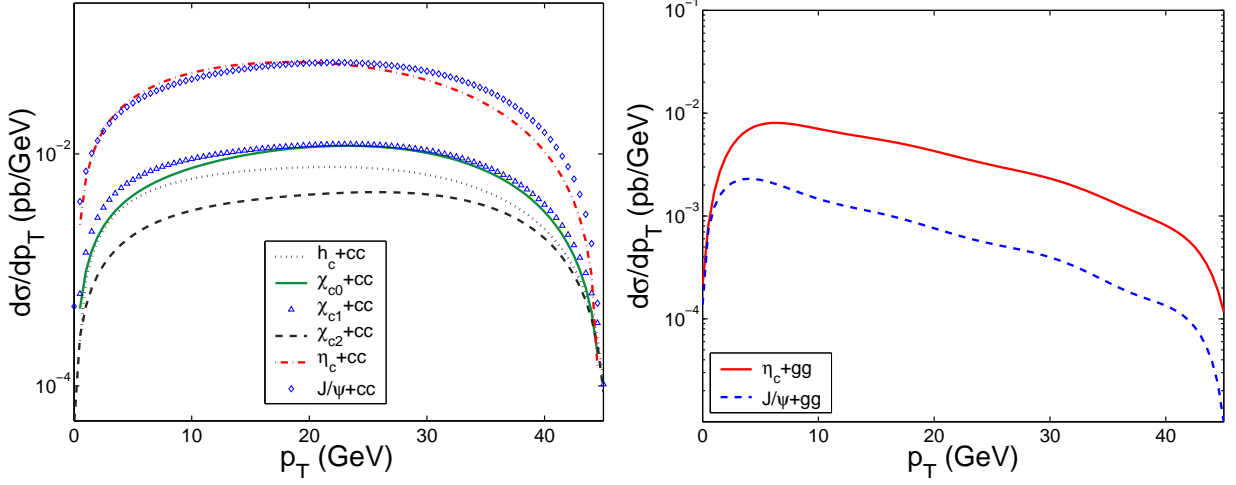


FIG. 10: The charmonium p_T distributions for the production processes $e^+e^- \rightarrow Z^0 \rightarrow |H_{c\bar{c}}\rangle + X$ at the e^+e^- collision energy $E_{cm} = m_Z$. The left panel is for $X = c\bar{c}$, the right one is for $X = gg$.

and

$$\frac{\sigma_{e^+e^- \rightarrow \gamma^* \rightarrow \Upsilon + b\bar{b}}}{\sigma_{e^+e^- \rightarrow Z^0 \rightarrow \Upsilon + b\bar{b}}} = 5.0 \times 10^{-4}.$$

To show this point clearly, we present the total cross sections for the color-singlet channels versus the collision energy E_{cm} in Figs. 6, 7, 8 and 9. In the low collision energy region, the production cross sections are dominated by the cases via the γ^* propagator, whose main contributions are around 6–20 GeV for charmonium production and 10–40 GeV for bottomonium production. The production via Z^0 propagator is small in the low energy region, but has a peak value at $E_{cm} = m_Z$ due to the Z^0 -boson resonance effect.

For the charmonium production channels, from Fig. 7 and Fig. 9, it is found that the total cross sections for $e^+e^- \rightarrow Z^0 \rightarrow J/\psi + c\bar{c}$ and $e^+e^- \rightarrow Z^0 \rightarrow \eta_c + c\bar{c}$, and the total cross sections for $e^+e^- \rightarrow Z^0 \rightarrow \chi_{c0} + c\bar{c}$ and $e^+e^- \rightarrow Z^0 \rightarrow \chi_{c1} + c\bar{c}$ are almost coincident with each other, especially for larger collision energy. The conditions for the bottomonium cases are similar. This shows that there is approximate “spin degeneracy” for the production channels $e^+e^- \rightarrow Z^0 \rightarrow |H_{Q\bar{Q}}\rangle + Q\bar{Q}$. Quantitatively, when the collision energy $E_{cm} = m_Z$, we have

$$\frac{\sigma_{e^+e^- \rightarrow Z^0 \rightarrow \eta_c + c\bar{c}}}{\sigma_{e^+e^- \rightarrow Z^0 \rightarrow J/\psi + c\bar{c}}} \simeq 96\%, \quad (43)$$

$$\frac{\sigma_{e^+e^- \rightarrow Z^0 \rightarrow \chi_{c0} + c\bar{c}}}{\sigma_{e^+e^- \rightarrow Z^0 \rightarrow \chi_{c1} + c\bar{c}}} \simeq 91\%, \quad (44)$$

$$\frac{\sigma_{e^+e^- \rightarrow Z^0 \rightarrow \eta_b + b\bar{b}}}{\sigma_{e^+e^- \rightarrow Z^0 \rightarrow \Upsilon + b\bar{b}}} \simeq 89\%, \quad (45)$$

$$\frac{\sigma_{e^+e^- \rightarrow Z^0 \rightarrow \chi_{b1} + b\bar{b}}}{\sigma_{e^+e^- \rightarrow Z^0 \rightarrow \chi_{b0} + b\bar{b}}} \simeq 95\%. \quad (46)$$

We present the heavy quarkonium transverse momentum (p_T) distributions and rapidity (y) distributions for $E_{cm} = m_Z$ in Figs. 10, 11, 12 and 13. These figures show that both for the p_T distributions and for the y distributions, the two curves for $e^+e^- \rightarrow Z^0 \rightarrow J/\psi + c\bar{c}$ and $e^+e^- \rightarrow Z^0 \rightarrow \eta_c + c\bar{c}$, and the two curves for $e^+e^- \rightarrow Z^0 \rightarrow \chi_{c0} + c\bar{c}$ and $e^+e^- \rightarrow Z^0 \rightarrow \chi_{c1} + c\bar{c}$ are very close to each other. The curves for the bottomonium production are similar.

As a cross check / explanation for the approximate “spin degeneracy”, we adopt the fragmentation approach. Using the fragmentation approach the most important/dominant higher-order effects can be included by using the Dokshitzer-Gribov-Lipatov-Altarelli-Parisi evolution equation, and the fragmentation approach gives a reasonable approximation to the full tree-level calculation as long as the transverse momentum of the produced heavy hadron is large enough [48–60]. Moreover, it has been argued that the fragmentation approach may be extended to lower p_T region under the FONLL scheme [61, 62].

In the large p_T region, the probabilities of $Z^0 \rightarrow J/\psi$ and $Z^0 \rightarrow \eta_c$ are proportional to each other and dominated by the fragmentations $c \rightarrow J/\psi$ and $c \rightarrow \eta_c$, respectively. To calculate them, we need to deal with the Feynman diagrams shown in Fig. 14 for the J/ψ case. With the choice of the axial gauge, the amplitudes of Figs. 14b and 14d

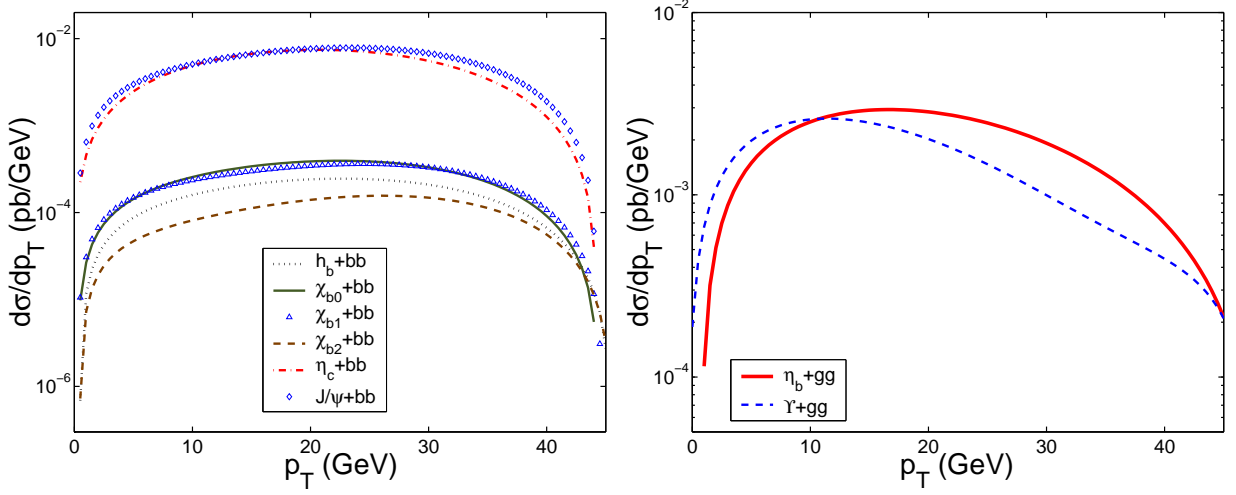


FIG. 11: The bottomonium p_T distributions for the production processes $e^+e^- \rightarrow Z^0 \rightarrow |H_{b\bar{b}}\rangle + X$ at the e^+e^- collision energy $E_{cm} = m_Z$. The left panel is for $X = b\bar{b}$, the right one is for $X = gg$.

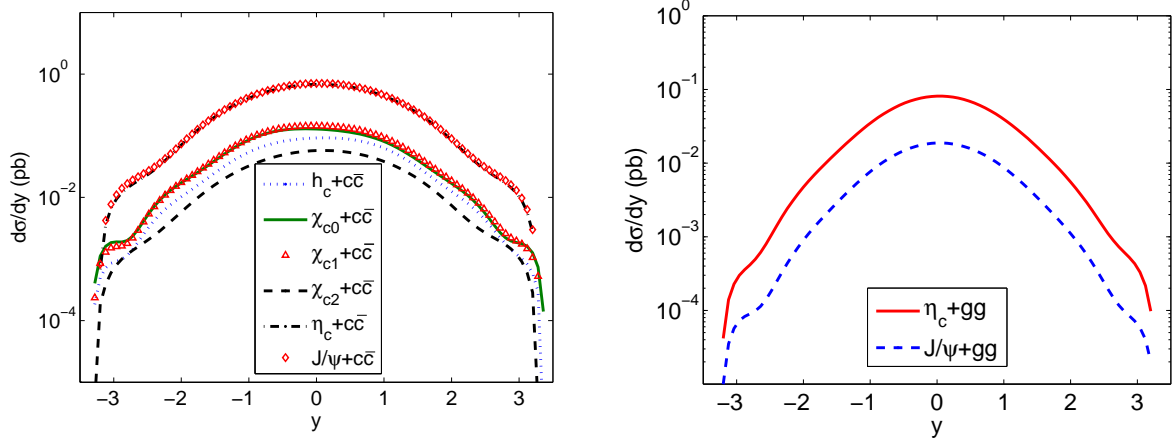


FIG. 12: The charmonium y distributions for the production processes $e^+e^- \rightarrow Z^0 \rightarrow |H_{c\bar{c}}\rangle + X$ at the e^+e^- collision energy $E_{cm} = m_Z$. The left panel is for $X = c\bar{c}$, the right one is for $X = gg$.

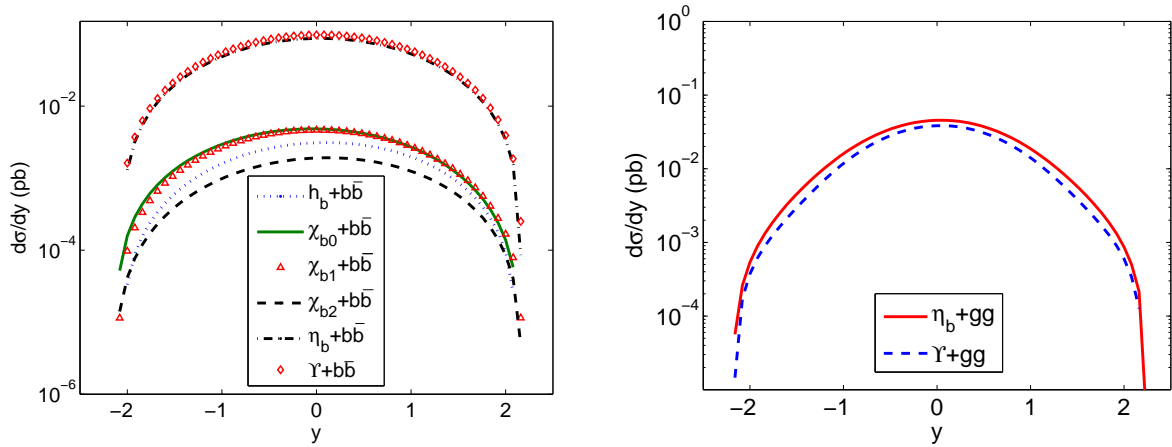


FIG. 13: The bottomonium y distributions for the production processes $e^+e^- \rightarrow Z^0 \rightarrow |H_{b\bar{b}}\rangle + X$ at the e^+e^- collision energy $E_{cm} = m_Z$. The left panel is for $X = b\bar{b}$, the right one is for $X = gg$.

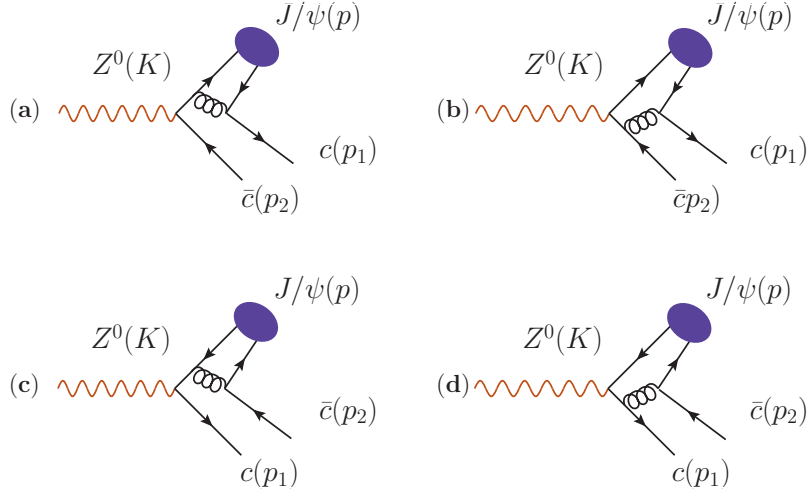


FIG. 14: Feynman diagrams for calculating the total fragmentation probabilities for $c \rightarrow J/\psi$ and $c \rightarrow \eta_c$.

are suppressed by a factor m_c/m_Z in comparison to those of Figs. 14a and 14c and they are, therefore, neglected in deriving the fragmentation probabilities for $c \rightarrow J/\psi$ and $c \rightarrow \eta_c$. Following the same procedure as shown by Ref.[58], one can obtain the total fragmentation probabilities:

$$\int_0^1 dz D_{c \rightarrow J/\psi}(z, 3m_c) = \frac{256}{27} \alpha_s (3m_c)^2 \times \frac{|\Psi_{1S}(0)|^2}{M_{J/\psi}^3} \left(\frac{1189}{30} - 57 \ln 2 \right), \quad (47)$$

$$\int_0^1 dz D_{c \rightarrow \eta_c}(z, 3m_c) = \frac{256}{27} \alpha_s (3m_c)^2 \times \frac{|\Psi_{1S}(0)|^2}{M_{\eta_c}^3} \left(\frac{773}{30} - 37 \ln 2 \right). \quad (48)$$

Then, the ratio of the two fragmentation probabilities is

$$\frac{\int_0^1 dz D_{c \rightarrow J/\psi}(z, 3m_c)}{\int_0^1 dz D_{c \rightarrow \eta_c}(z, 3m_c)} \simeq 97\%.$$

This is consistent with Eq.(43) and confirms that there is spin-degeneracy for e^+e^- at the high collision energy. The total fragmentation probabilities for $b \rightarrow \Upsilon$ and $b \rightarrow \eta_b$ can be obtained from these expressions by replacing m_c with m_b . The probabilities for P -wave production can be derived in a similar way, obtaining the results found in Ref.[60], which we confirm with our calculations.

In real experiments, due to the limited detector sensitivity and acceptance, events with small p_T and/or large $|y|$ may not be detected. To account for this effect, we report in Tables IV, V, VI and VII the cross sections with different cuts on the variables p_T and $|y|$.

2. Uncertainties from the determinations of E_{cm} and m_Q

For the leading-order calculation, the uncertainty sources include the bound-state matrix elements, the renormalization scale, the quark masses m_b and m_c . The conventional scale setting assigns the typical momentum flow of the process as the renormalization scale, e.g. $2m_c$ for charmonium production and $2m_b$ for bottomonium production. This rough assignment of scale and its range leads to an important systematic error in the present theoretical estimations. In the literature, the principle of maximum conformality (PMC) [63] provides a feasible way to derive precise QCD predictions. The main idea of PMC is to sum all the non-conformal β -terms in the perturbative expansion into the running coupling. The remaining terms are then identical to that of a conformal theory. The PMC estimation is then

Channel	$p_T > 5$ GeV	$p_T > 10$ GeV	$p_T > 15$ GeV
$\sigma_{J/\psi(1S)+c\bar{c}}$	1.75(96%)	1.55(85%)	1.29(70%)
$\sigma_{\psi'(2S)+c\bar{c}}$	1.11(96%)	9.81×10^{-1} (85%)	8.17×10^{-1} (70%)
$\sigma_{J/\psi(1S)+gg}$	2.89×10^{-2} (75%)	1.96×10^{-2} (51%)	1.30×10^{-2} (34%)
$\sigma_{\psi'(2S)+gg}$	1.83×10^{-2} (75%)	1.24×10^{-2} (51%)	8.23×10^{-3} (34%)
$\sigma_{\eta_c(1S)+c\bar{c}}$	1.68(95%)	1.46(83%)	1.17(66%)
$\sigma_{\eta'_c(2S)+c\bar{c}}$	1.06(95%)	9.24×10^{-1} (83%)	7.41×10^{-1} (66%)
$\sigma_{\eta_c(1S)+gg}$	1.47×10^{-1} (85%)	1.08×10^{-1} (63%)	7.51×10^{-2} (44%)
$\sigma_{\eta'_c(2S)+gg}$	9.31×10^{-2} (85%)	6.84×10^{-2} (63%)	4.75×10^{-2} (44%)
$\sigma_{h_c(1P)+c\bar{c}}$	2.22×10^{-1} (95%)	1.96×10^{-1} (84%)	1.61×10^{-1} (69%)
$\sigma_{\chi_{c0}(1P)+c\bar{c}}$	3.17×10^{-1} (95%)	2.86×10^{-1} (86%)	2.42×10^{-1} (73%)
$\sigma_{\chi_{c1}(1P)+c\bar{c}}$	3.46×10^{-1} (94%)	3.08×10^{-1} (84%)	2.56×10^{-1} (70%)
$\sigma_{\chi_{c2}(1P)+c\bar{c}}$	1.37×10^{-1} (95%)	1.24×10^{-1} (86%)	1.05×10^{-1} (73%)

TABLE IV: Cross section (in pb) for the color-singlet charmonium production with different p_T cuts. The channels are through Z^0 propagator for $\sqrt{s} = m_Z$ and $m_c=1.5$ GeV. The percentages in the parentheses represent the ratios between the cross section with and without p_T cut.

Channel	$p_T > 5$ GeV	$p_T > 10$ GeV	$p_T > 15$ GeV
$\sigma_{\Upsilon(1S)+b\bar{b}}$	2.10×10^{-1} (96%)	1.89×10^{-1} (87%)	1.59×10^{-1} (73%)
$\sigma_{\Upsilon'(2S)+b\bar{b}}$	1.04×10^{-1} (96%)	9.35×10^{-2} (87%)	7.86×10^{-2} (73%)
$\sigma_{\Upsilon(1S)+gg}$	5.90×10^{-2} (90%)	4.63×10^{-2} (71%)	3.37×10^{-2} (51%)
$\sigma_{\Upsilon'(2S)+gg}$	2.92×10^{-2} (90%)	2.29×10^{-2} (71%)	1.67×10^{-2} (51%)
$\sigma_{\eta_b(1S)+b\bar{b}}$	1.88×10^{-1} (97%)	1.68×10^{-1} (87%)	1.38×10^{-1} (71%)
$\sigma_{\eta'_b(2S)+b\bar{b}}$	9.30×10^{-2} (97%)	8.31×10^{-2} (87%)	6.83×10^{-2} (71%)
$\sigma_{\eta_b(1S)+gg}$	7.85×10^{-2} (96%)	6.80×10^{-2} (83%)	5.35×10^{-2} (65%)
$\sigma_{\eta'_b(2S)+gg}$	3.88×10^{-2} (96%)	3.36×10^{-2} (83%)	2.65×10^{-2} (65%)
$\sigma_{h_b(1P)+b\bar{b}}$	6.60×10^{-3} (96%)	6.00×10^{-3} (88%)	5.00×10^{-3} (73%)
$\sigma_{\chi_{b0}(1P)+b\bar{b}}$	1.05×10^{-2} (96%)	9.40×10^{-3} (86%)	7.85×10^{-3} (72%)
$\sigma_{\chi_{b1}(1P)+b\bar{b}}$	9.95×10^{-3} (96%)	8.95×10^{-3} (86%)	7.60×10^{-3} (73%)
$\sigma_{\chi_{b2}(1P)+b\bar{b}}$	4.16×10^{-3} (97%)	3.84×10^{-3} (89%)	3.33×10^{-3} (77%)

TABLE V: Cross section (in pb) for the color-singlet bottomonium production with different p_T cuts. The channels are through Z^0 propagator for $\sqrt{s} = m_Z$ and $m_b=4.9$ GeV. The percentages in the parentheses represent the ratios between the cross section with and without p_T cut.

scheme independent, and the remaining scale dependence is greatly suppressed. In the present framework, the matrix elements and the strong coupling constant α_s emerge as overall factors and their uncertainties can be conveniently discussed, so we will not discuss their uncertainties in the present paper.

As shown in the last subsection, if the collision energy E_{cm} is around m_Z , the total cross sections for the channels via the γ^* propagator are much smaller than those of the channels via the Z^0 propagator. In the present subsection we address the production via Z^0 propagator, i.e. the channel $e^+e^- \rightarrow Z^0 \rightarrow |H_{Q\bar{Q}}\rangle + X$. For clarity, when we discuss the uncertainty due to a given parameter we fix all others to their central values.

To show the sensitivity of the total cross sections to the collision energy around the Z^0 peak, we calculate the total cross sections by taking $E_{cm} = (1 \pm 3\%)m_Z$. Our results are presented in Tables VIII and IX, where we define two ratios

$$R_- = \frac{\sigma(E_{cm} = 97\%m_Z)}{\sigma(E_{cm} = m_Z)}$$

and

$$R_+ = \frac{\sigma(E_{cm} = 103\%m_Z)}{\sigma(E_{cm} = m_Z)}$$

Channel	$ y < 0.5$	$ y < 1.0$	$ y < 1.5$
$\sigma_{J/\psi(1S)+c\bar{c}}$	7.00×10^{-1} (38%)	1.27(69%)	1.60(87%)
$\sigma_{\psi'(2S)+c\bar{c}}$	4.43×10^{-1} (38%)	8.04×10^{-1} (69%)	1.01(87%)
$\sigma_{J/\psi(1S)+gg}$	1.82×10^{-2} (47%)	3.02×10^{-2} (79%)	3.58×10^{-2} (93%)
$\sigma_{\psi'(2S)+gg}$	1.15×10^{-2} (47%)	1.91×10^{-2} (79%)	2.27×10^{-2} (93%)
$\sigma_{\eta_c(1S)+c\bar{c}}$	6.71×10^{-1} (38%)	1.23(70%)	1.55(88%)
$\sigma_{\eta'_c(2S)+c\bar{c}}$	4.25×10^{-1} (38%)	7.79×10^{-1} (70%)	9.81×10^{-1} (88%)
$\sigma_{\eta_c(1S)+gg}$	7.88×10^{-2} (46%)	1.32×10^{-1} (77%)	1.58×10^{-1} (92%)
$\sigma_{\eta'_c(2S)+gg}$	4.99×10^{-2} (46%)	8.36×10^{-2} (77%)	1.00×10^{-1} (92%)
$\sigma_{h_c(1P)+c\bar{c}}$	8.97×10^{-2} (38%)	1.63×10^{-1} (70%)	2.05×10^{-1} (88%)
$\sigma_{\chi_{c0}(1P)+c\bar{c}}$	1.25×10^{-1} (38%)	2.28×10^{-1} (68%)	2.88×10^{-1} (86%)
$\sigma_{\chi_{c1}(1P)+c\bar{c}}$	1.39×10^{-1} (38%)	2.53×10^{-1} (69%)	3.20×10^{-1} (87%)
$\sigma_{\chi_{c2}(1P)+c\bar{c}}$	5.48×10^{-2} (38%)	9.97×10^{-2} (69%)	1.25×10^{-1} (87%)

TABLE VI: Cross section (in pb) for the color-singlet charmonium production with different y cuts. The channels are through Z^0 propagator for $\sqrt{s} = m_Z$ and $m_c=1.5$ GeV. The percentages in the parentheses represent the ratios between the cross sections with and without rapidity cut.

Channel	$ y < 0.5$	$ y < 1.0$	$ y < 1.5$
$\sigma_{\Upsilon(1S)+b\bar{b}}$	9.40×10^{-2} (43%)	1.67×10^{-1} (77%)	2.06×10^{-1} (94%)
$\sigma_{\Upsilon'(2S)+b\bar{b}}$	4.65×10^{-2} (43%)	8.26×10^{-2} (77%)	1.02×10^{-1} (94%)
$\sigma_{\Upsilon(1S)+gg}$	3.54×10^{-2} (54%)	5.63×10^{-2} (86%)	6.38×10^{-2} (98%)
$\sigma_{\Upsilon'(2S)+gg}$	1.75×10^{-2} (54%)	2.78×10^{-2} (86%)	3.16×10^{-2} (98%)
$\sigma_{\eta_b(1S)+b\bar{b}}$	8.26×10^{-2} (43%)	1.49×10^{-1} (77%)	1.84×10^{-1} (95%)
$\sigma_{\eta'_b(2S)+b\bar{b}}$	4.09×10^{-2} (43%)	7.37×10^{-2} (77%)	9.10×10^{-2} (95%)
$\sigma_{\eta_b(1S)+gg}$	4.23×10^{-2} (52%)	6.87×10^{-2} (84%)	7.92×10^{-2} (97%)
$\sigma_{\eta'_b(2S)+gg}$	2.09×10^{-2} (52%)	3.40×10^{-2} (84%)	3.92×10^{-2} (97%)
$\sigma_{h_b(1P)+b\bar{b}}$	3.01×10^{-3} (44%)	5.29×10^{-3} (77%)	6.48×10^{-3} (95%)
$\sigma_{\chi_{b0}(1P)+b\bar{b}}$	4.60×10^{-3} (42%)	8.26×10^{-3} (76%)	1.02×10^{-2} (94%)
$\sigma_{\chi_{b1}(1P)+b\bar{b}}$	4.47×10^{-3} (43%)	7.93×10^{-3} (76%)	9.77×10^{-3} (94%)
$\sigma_{\chi_{b2}(1P)+b\bar{b}}$	1.84×10^{-3} (43%)	3.27×10^{-3} (76%)	4.02×10^{-3} (93%)

TABLE VII: Cross section (in pb) for the color-singlet bottomonium production with different y cuts. The channels are through Z^0 propagator for $\sqrt{s} = m_Z$ and $m_b=4.9$ GeV. The percentages in the parentheses represent the ratios between the cross sections with and without rapidity cut.

to show how the cross sections are changed with varying values of E_{cm} . For example, by varying E_{cm} within this range, the total cross sections for the production of J/ψ and Υ drop to 16 – 18% of their peak values.

Next, we discuss the uncertainties from the heavy quark masses by varying $m_c = 1.50 \pm 0.15$ GeV and $m_b = 4.9 \pm 0.15$ GeV respectively. Our results for $e^+e^- \rightarrow Z^0 \rightarrow |H_{Q\bar{Q}}\rangle + X$ are presented in Tables X and XI. The tables show that

- for charmonium production, with $X = c\bar{c}$, the uncertainties associated with the variation $m_c = 1.50 \pm 0.15$ GeV are $\sim 40\%$ for the S -wave case and 70% for the P -wave case; for $X = gg$, the uncertainty are $\sim 15\% - 19\%$.
- for bottomonium production, with $X = b\bar{b}$, the uncertainties associated with the variation $m_b = 4.90 \pm 0.15$ GeV are $\sim 11\%$ for the S -wave case and $15\% - 18\%$ for the P -wave case; for $X = gg$, the uncertainties are $\sim 6\%$.

Channel	$E_{cm} = 97\%m_Z$	$E_{cm} = 103\%m_Z$	$\left(\frac{R_-}{R_+}\right)$
$\sigma_{\eta_c+c\bar{c}}$	2.91×10^{-1}	3.14×10^{-1}	$\left(\frac{17\%}{18\%}\right)$
$\sigma_{\eta'_c+c\bar{c}}$	1.84×10^{-1}	1.99×10^{-1}	$\left(\frac{17\%}{18\%}\right)$
$\sigma_{J/\psi+c\bar{c}}$	3.02×10^{-1}	3.26×10^{-1}	$\left(\frac{17\%}{18\%}\right)$
$\sigma_{\psi'+c\bar{c}}$	1.91×10^{-1}	2.06×10^{-1}	$\left(\frac{17\%}{18\%}\right)$
$\sigma_{J/\psi+gg}$	6.66×10^{-3}	6.57×10^{-3}	$\left(\frac{17\%}{17\%}\right)$
$\sigma_{\psi'+gg}$	4.22×10^{-3}	4.16×10^{-3}	$\left(\frac{17\%}{17\%}\right)$
σ_{η_c+gg}	2.97×10^{-2}	2.94×10^{-2}	$\left(\frac{17\%}{17\%}\right)$
$\sigma_{\eta'_c+gg}$	1.88×10^{-2}	1.86×10^{-2}	$\left(\frac{17\%}{17\%}\right)$
$\sigma_{h_c+c\bar{c}}$	3.88×10^{-2}	4.18×10^{-2}	$\left(\frac{17\%}{18\%}\right)$
$\sigma_{\chi_{c0}+c\bar{c}}$	5.51×10^{-2}	5.92×10^{-2}	$\left(\frac{17\%}{18\%}\right)$
$\sigma_{\chi_{c1}+c\bar{c}}$	6.08×10^{-2}	6.55×10^{-2}	$\left(\frac{17\%}{18\%}\right)$
$\sigma_{\chi_{c2}+c\bar{c}}$	2.40×10^{-2}	2.59×10^{-2}	$\left(\frac{17\%}{18\%}\right)$

TABLE VIII: Total cross sections (in pb) for the production channels $e^+e^- \rightarrow Z^0 \rightarrow |H_{c\bar{c}}\rangle + X$, with varying values of E_{cm} . The ratios R_{\mp} in the last column show how the cross sections are changed with varying values of E_{cm} .

Channel	$E_{cm} = 97\%m_Z$	$E_{cm} = 103\%m_Z$	$\left(\frac{R_-}{R_+}\right)$
$\sigma_{\eta_b+b\bar{b}}$	3.17×10^{-2}	3.53×10^{-2}	$\left(\frac{16\%}{18\%}\right)$
$\sigma_{\eta'_b+b\bar{b}}$	1.57×10^{-2}	1.75×10^{-2}	$\left(\frac{16\%}{18\%}\right)$
$\sigma_{\Upsilon+b\bar{b}}$	3.57×10^{-2}	3.95×10^{-2}	$\left(\frac{16\%}{18\%}\right)$
$\sigma_{\Upsilon'+b\bar{b}}$	1.77×10^{-2}	1.95×10^{-2}	$\left(\frac{16\%}{18\%}\right)$
$\sigma_{\Upsilon+gg}$	1.12×10^{-2}	1.13×10^{-2}	$\left(\frac{17\%}{17\%}\right)$
$\sigma_{\Upsilon'+gg}$	5.54×10^{-3}	5.59×10^{-3}	$\left(\frac{17\%}{17\%}\right)$
σ_{η_b+gg}	1.40×10^{-2}	1.42×10^{-2}	$\left(\frac{17\%}{17\%}\right)$
$\sigma_{\eta'_b+gg}$	6.93×10^{-3}	7.03×10^{-3}	$\left(\frac{17\%}{17\%}\right)$
$\sigma_{h_b+b\bar{b}}$	1.13×10^{-3}	1.24×10^{-3}	$\left(\frac{16\%}{18\%}\right)$
$\sigma_{\chi_{b0}+b\bar{b}}$	1.80×10^{-3}	1.95×10^{-3}	$\left(\frac{16\%}{18\%}\right)$
$\sigma_{\chi_{b1}+b\bar{b}}$	1.71×10^{-3}	1.88×10^{-3}	$\left(\frac{16\%}{18\%}\right)$
$\sigma_{\chi_{b2}+b\bar{b}}$	7.06×10^{-4}	7.74×10^{-4}	$\left(\frac{16\%}{18\%}\right)$

TABLE IX: Total cross sections (in pb) for the production channels $e^+e^- \rightarrow Z^0 \rightarrow |H_{b\bar{b}}\rangle + X$, with varying values of E_{cm} . The ratios R_{\mp} in the last column show how the cross sections are changed with varying values of E_{cm} .

B. Properties of the color-octet processes

1. Total cross sections

As discussed in the introduction, we will consider the following sizeable color-octet processes

$$\begin{aligned}
e^+e^- \rightarrow Z^0 &\rightarrow |(Q\bar{Q})[(1^1S_0^{(8)}), (1^3S_1^{(8)})]g\rangle + Q\bar{Q} \\
&\rightarrow \psi_Q + Q\bar{Q}, \\
e^+e^- \rightarrow Z^0 &\rightarrow |(Q\bar{Q})[(1^1S_0^{(8)})]g\rangle + Q\bar{Q} \rightarrow h_Q + Q\bar{Q}, \\
e^+e^- \rightarrow Z^0 &\rightarrow |(Q\bar{Q})[(1^3S_1^{(8)})]g\rangle + Q\bar{Q} \rightarrow \chi_{QJ} + Q\bar{Q}
\end{aligned}$$

and

$$e^+e^- \rightarrow Z^0 \rightarrow |(Q\bar{Q})[(1^1S_0^{(8)}), (1^3S_1^{(8)})]g\rangle + g,$$

m_c GeV	1.35 GeV	1.65 GeV	uncertainty
$\sigma_{\eta_c+c\bar{c}}$	2.44	1.31	+0.680 -0.450
$\sigma_{\eta'_c+c\bar{c}}$	1.54	8.29×10^{-1}	+0.430 -0.281
$\sigma_{J/\psi+c\bar{c}}$	2.53	1.36	+0.700 -0.470
$\sigma_{\psi'+c\bar{c}}$	1.60	8.61×10^{-1}	+0.440 -0.299
$\sigma_{J/\psi+gg}$	4.55×10^{-2}	3.29×10^{-2}	+0.007 -0.006
$\sigma_{\psi'+gg}$	2.88×10^{-2}	2.08×10^{-2}	+0.005 -0.004
σ_{η_c+gg}	2.04×10^{-1}	1.46×10^{-1}	+0.032 -0.026
$\sigma_{\eta'_c+gg}$	1.29×10^{-1}	9.24×10^{-2}	+0.020 -0.017
$\sigma_{h_c+c\bar{c}}$	3.99×10^{-1}	1.45×10^{-1}	+0.165 -0.089
$\sigma_{\chi_{c0}+c\bar{c}}$	5.64×10^{-1}	2.04×10^{-1}	+0.232 -0.128
$\sigma_{\chi_{c1}+c\bar{c}}$	6.25×10^{-1}	2.26×10^{-1}	+0.259 -0.140
$\sigma_{\chi_{c2}+c\bar{c}}$	2.44×10^{-1}	8.90×10^{-2}	+0.100 -0.055

TABLE X: Total cross sections (in pb) for the channels $e^+e^- \rightarrow Z^0 \rightarrow |H_{c\bar{c}}\rangle + X$ with varying values of m_c . The uncertainties in the last column are the deviations from the central values corresponding to $m_c = 1.5$ GeV.

m_b (GeV)	4.75GeV	5.05GeV	uncertainty
$\sigma_{\eta_b+b\bar{b}}$	2.17×10^{-1}	1.74×10^{-1}	+0.023 -0.020
$\sigma_{\eta'_b+b\bar{b}}$	1.07×10^{-1}	8.61×10^{-2}	+0.011 -0.010
$\sigma_{\Upsilon+b\bar{b}}$	2.43×10^{-1}	1.96×10^{-1}	+0.025 -0.022
$\sigma_{\Upsilon'+b\bar{b}}$	1.20×10^{-1}	9.70×10^{-2}	+0.012 -0.011
$\sigma_{\Upsilon+gg}$	6.95×10^{-2}	6.17×10^{-2}	+0.004 -0.003
$\sigma_{\Upsilon'+gg}$	3.44×10^{-2}	3.05×10^{-2}	+0.002 -0.002
σ_{η_b+gg}	8.72×10^{-2}	7.69×10^{-2}	+0.005 -0.005
$\sigma_{\eta'_b+gg}$	4.32×10^{-2}	3.81×10^{-2}	+0.003 -0.002
$\sigma_{h_b+b\bar{b}}$	8.12×10^{-3}	5.83×10^{-3}	+0.001 -0.001
$\sigma_{\chi_{b0}+b\bar{b}}$	1.28×10^{-2}	9.31×10^{-3}	+0.002 -0.002
$\sigma_{\chi_{b1}+b\bar{b}}$	1.23×10^{-2}	8.87×10^{-3}	+0.002 -0.002
$\sigma_{\chi_{b2}+b\bar{b}}$	5.09×10^{-3}	3.67×10^{-3}	+0.001 -0.001

TABLE XI: Total cross sections (in pb) for the channels $e^+e^- \rightarrow Z^0 \rightarrow |H_{b\bar{b}}\rangle + X$ with varying values of m_b GeV. The uncertainties in the last column are the deviations from the central values corresponding to $m_b = 4.9$ GeV.

$$\begin{aligned}
& \rightarrow \psi_Q + g \\
e^+e^- \rightarrow Z^0 & \rightarrow |(Q\bar{Q})[(1^1S_0^{(8)})]g\rangle + g \rightarrow h_Q + g, \\
e^+e^- \rightarrow Z^0 & \rightarrow |(Q\bar{Q})[(1^3S_1^{(8)})]g\rangle + g \rightarrow \chi_{QJ} + g.
\end{aligned}$$

It is noted that the total cross sections for the color-octet channels versus the collision energy have similar shapes to those in Figs. 6, 7, 8 and 9. We present their total cross sections at the e^+e^- collision energy $E_{cm} = \sqrt{s} = m_Z$ in Tables XII and XIII. For the channels with $X = c\bar{c}$ or $b\bar{b}$, the results in these tables, compared to those in Tables II and III, imply

$$\begin{aligned}
& \frac{\sigma(e^+e^- \rightarrow Z^0 \rightarrow |(c\bar{c})[(1^1S_0^{(8)})]g\rangle + c\bar{c} \rightarrow J/\psi + c\bar{c})}{\sigma(e^+e^- \rightarrow Z^0 \rightarrow |(c\bar{c})[(1^3S_1^{(1)})]g\rangle + c\bar{c} \rightarrow J/\psi + c\bar{c})} = 0.1\%, \\
& \frac{\sigma(e^+e^- \rightarrow Z^0 \rightarrow |(c\bar{c})[(1^3S_1^{(8)})]g\rangle + c\bar{c} \rightarrow J/\psi + c\bar{c})}{\sigma(e^+e^- \rightarrow Z^0 \rightarrow |(c\bar{c})[(1^3S_1^{(1)})]g\rangle + c\bar{c} \rightarrow J/\psi + c\bar{c})} = 50\%, \\
& \frac{\sigma(e^+e^- \rightarrow Z^0 \rightarrow |(b\bar{b})[(1^1S_0^{(8)})]g\rangle + b\bar{b} \rightarrow \Upsilon + b\bar{b})}{\sigma(e^+e^- \rightarrow Z^0 \rightarrow |(b\bar{b})[(1^3S_1^{(1)})]g\rangle + b\bar{b} \rightarrow \Upsilon + b\bar{b})} = 0.01\%,
\end{aligned}$$

J/ψ or Υ production channels	$\sigma_{(a)}$	$\sigma_{(b)}$	$\sigma_{(c)}$	σ_{tot}
$e^+e^- \rightarrow Z^0 \rightarrow (c\bar{c})[(1^1S_0^{(8)})]g\rangle + c\bar{c} \rightarrow J/\psi + c\bar{c}$	1.65×10^{-3}	2.65×10^{-5}	\sim	1.69×10^{-3}
$e^+e^- \rightarrow Z^0 \rightarrow (c\bar{c})[(1^3S_1^{(8)})]g\rangle + c\bar{c} \rightarrow J/\psi + c\bar{c}$	1.71×10^{-3}	1.80×10^{-4}	8.92×10^{-1}	9.11×10^{-1}
$e^+e^- \rightarrow Z^0 \rightarrow (c\bar{c})[(1^1S_0^{(8)})]g\rangle + g \rightarrow J/\psi + g$	\sim	\sim	\sim	4.87×10^{-4}
$e^+e^- \rightarrow Z^0 \rightarrow (c\bar{c})[(1^3S_1^{(8)})]g\rangle + g \rightarrow J/\psi + g$	\sim	\sim	\sim	3.31×10^{-3}
$e^+e^- \rightarrow Z^0 \rightarrow (b\bar{b})[(1^1S_0^{(8)})]g\rangle + b\bar{b} \rightarrow \Upsilon + b\bar{b}$	1.86×10^{-5}	5.22×10^{-6}	\sim	2.76×10^{-5}
$e^+e^- \rightarrow Z^0 \rightarrow (b\bar{b})[(1^3S_1^{(8)})]g\rangle + b\bar{b} \rightarrow \Upsilon + b\bar{b}$	2.09×10^{-5}	1.13×10^{-5}	4.05×10^{-3}	4.23×10^{-3}
$e^+e^- \rightarrow Z^0 \rightarrow (b\bar{b})[(1^1S_0^{(8)})]g\rangle + g \rightarrow \Upsilon + g$	\sim	\sim	\sim	2.81×10^{-4}
$e^+e^- \rightarrow Z^0 \rightarrow (b\bar{b})[(1^3S_1^{(8)})]g\rangle + g \rightarrow \Upsilon + g$	\sim	\sim	\sim	5.93×10^{-4}

TABLE XII: Total cross sections (in pb) for the color-octet heavy quarkonium production via the e^+e^- annihilation at $\sqrt{s} = m_Z$, where the subscripts (a), (b) and (c) refer to the Feynman diagrams shown in the corresponding panels of Figs.3 and 4 respectively. The symbol σ_{tot} refers to the sum of $\sigma_{(a)}$, $\sigma_{(b)}$, $\sigma_{(c)}$ and their interference terms for the channel $e^+e^- \rightarrow Z^0 \rightarrow |(Q\bar{Q})[(1^1S_0^{(8)})], (1^3S_1^{(8)})]g\rangle + Q\bar{Q}$, and to the cross section of Fig.5 for the channel $e^+e^- \rightarrow Z^0 \rightarrow |(Q\bar{Q})[(1^1S_0^{(8)})], (1^3S_1^{(8)})]g\rangle + g$.

$h_c(h_b)$ or $\chi_{cJ}(\chi_{bJ})$ production channels	$\sigma_{(a)}$	$\sigma_{(b)}$	$\sigma_{(c)}$	σ_{tot}
$e^+e^- \rightarrow Z^0 \rightarrow (c\bar{c})[(1^1S_0^{(8)})]g\rangle + c\bar{c} \rightarrow h_c + c\bar{c}$	6.59×10^{-3}	1.06×10^{-4}	\sim	6.78×10^{-3}
$e^+e^- \rightarrow Z^0 \rightarrow (c\bar{c})[(1^3S_1^{(8)})]g\rangle + c\bar{c} \rightarrow \chi_{cJ} + c\bar{c}$	6.85×10^{-3}	7.21×10^{-4}	3.56	3.65
$e^+e^- \rightarrow Z^0 \rightarrow (c\bar{c})[(1^1S_0^{(8)})]g\rangle + g \rightarrow h_c + g$	\sim	\sim	\sim	1.95×10^{-3}
$e^+e^- \rightarrow Z^0 \rightarrow (c\bar{c})[(1^3S_1^{(8)})]g\rangle + g \rightarrow \chi_{cJ} + g$	\sim	\sim	\sim	1.32×10^{-2}
$e^+e^- \rightarrow Z^0 \rightarrow (b\bar{b})[(1^1S_0^{(8)})]g\rangle + b\bar{b} \rightarrow h_b + b\bar{b}$	2.53×10^{-4}	7.09×10^{-5}	\sim	3.75×10^{-4}
$e^+e^- \rightarrow Z^0 \rightarrow (b\bar{b})[(1^3S_1^{(8)})]g\rangle + b\bar{b} \rightarrow \chi_{bJ} + b\bar{b}$	2.09×10^{-4}	1.53×10^{-4}	4.26×10^{-2}	4.44×10^{-2}
$e^+e^- \rightarrow Z^0 \rightarrow (b\bar{b})[(1^1S_0^{(8)})]g\rangle + g \rightarrow h_b + g$	\sim	\sim	\sim	3.81×10^{-3}
$e^+e^- \rightarrow Z^0 \rightarrow (b\bar{b})[(1^3S_1^{(8)})]g\rangle + g \rightarrow \chi_{bJ} + g$	\sim	\sim	\sim	8.05×10^{-3}

TABLE XIII: Total cross sections (in pb) for the color-octet heavy quarkonium production via the e^+e^- annihilation at $\sqrt{s} = m_Z$, where the subscripts (a), (b) and (c) refer to the Feynman figures shown in corresponding panel of Figs.3 and 4 respectively. The symbol σ_{tot} refers to the sum of $\sigma_{(a)}$, $\sigma_{(b)}$, $\sigma_{(c)}$ and their interference terms for the channel $e^+e^- \rightarrow Z^0 \rightarrow |(Q\bar{Q})[(1^1S_0^{(8)})], (1^3S_1^{(8)})]g\rangle + Q\bar{Q}$, and to the cross section of Fig.5 for the channel $e^+e^- \rightarrow Z^0 \rightarrow |(Q\bar{Q})[(1^1S_0^{(8)})], (1^3S_1^{(8)})]g\rangle + g$. Here the contributions to $^3P_0, ^3P_1, ^3P_2$ from the color-octet component $(Q\bar{Q})[(1^3S_1^{(8)})]g\rangle$ have been summed up.

$$\begin{aligned}
& \frac{\sigma(e^+e^- \rightarrow Z^0 \rightarrow |(b\bar{b})[(1^3S_1^{(8)})]g\rangle + b\bar{b} \rightarrow \Upsilon + b\bar{b})}{\sigma(e^+e^- \rightarrow Z^0 \rightarrow |(b\bar{b})[(1^3S_1^{(1)})]g\rangle + b\bar{b} \rightarrow \Upsilon + b\bar{b})} = 1.9\% \\
& \frac{\sigma(e^+e^- \rightarrow Z^0 \rightarrow |(c\bar{c})[(1^1S_0^{(8)})]g\rangle + c\bar{c} \rightarrow h_c + c\bar{c})}{\sigma(e^+e^- \rightarrow Z^0 \rightarrow |(c\bar{c})[(1^1P_1^{(1)})]g\rangle + c\bar{c} \rightarrow h_c + c\bar{c})} = 2.9\%, \\
& \frac{\sigma(e^+e^- \rightarrow Z^0 \rightarrow |(c\bar{c})[(1^3S_1^{(8)})]g\rangle + c\bar{c} \rightarrow \chi_{cJ} + c\bar{c})}{\sigma(e^+e^- \rightarrow Z^0 \rightarrow |(c\bar{c})[(1^3P_J^{(1)})]g\rangle + c\bar{c} \rightarrow \chi_{cJ} + c\bar{c})} = 433\%, \\
& \frac{\sigma(e^+e^- \rightarrow Z^0 \rightarrow |(b\bar{b})[(1^1S_0^{(8)})]g\rangle + b\bar{b} \rightarrow h_b + b\bar{b})}{\sigma(e^+e^- \rightarrow Z^0 \rightarrow |(b\bar{b})[(1^1P_1^{(1)})]g\rangle + b\bar{b} \rightarrow h_b + b\bar{b})} = 5.5\%, \\
& \frac{\sigma(e^+e^- \rightarrow Z^0 \rightarrow |(b\bar{b})[(1^3S_1^{(8)})]g\rangle + b\bar{b} \rightarrow \chi_{bJ} + b\bar{b})}{\sigma(e^+e^- \rightarrow Z^0 \rightarrow |(b\bar{b})[(1^3P_J^{(1)})]g\rangle + b\bar{b} \rightarrow \chi_{bJ} + b\bar{b})} = 173\%.
\end{aligned}$$

The analogous ratios for the cases $X = g$ have similar values.

We now discuss the relative importance of different channels for quarkonium production at the super Z factory with $E_{cm} = m_Z$ and at a B factory with $E_{cm} = 10.6$ GeV.

- At the super Z factory, the channel $e^+e^- \rightarrow Z^0 \rightarrow |(Q\bar{Q})[(1^3S_1^{(8)})]g\rangle + Q\bar{Q}$, with the topology shown in Fig. 4c, provides the dominant contribution with respect to other octet channels. A similar enhancement is not expected at the B factory, where quarkonium production is dominated by the γ^* propagator and, for example,

$$\frac{\sigma(e^+e^- \rightarrow \gamma^* \rightarrow |(c\bar{c})[(1^3S_1^{(8)})]g\rangle + c\bar{c} \rightarrow J/\psi + c\bar{c})}{\sigma(e^+e^- \rightarrow \gamma^* \rightarrow |(c\bar{c})[(1^3S_1^{(1)})]g\rangle + c\bar{c} \rightarrow J/\psi + c\bar{c})} \sim 3.1\%,$$

$$\frac{\sigma(e^+e^- \rightarrow \gamma^* \rightarrow |(c\bar{c})[(1^3S_1^{(8)})]g\rangle + c\bar{c} \rightarrow \chi_{cJ} + c\bar{c})}{\sigma(e^+e^- \rightarrow \gamma^* \rightarrow |(c\bar{c})[(1^3P_J^{(1)})]g\rangle + c\bar{c} \rightarrow \chi_{cJ} + c\bar{c})} \sim 19\%.$$

- At the super Z factory, the channels $e^+e^- \rightarrow Z^0 \rightarrow |(Q\bar{Q})[(1^1S_0^{(8)}), (1^3S_1^{(8)})]g\rangle + g$ are less important than $e^+e^- \rightarrow Z^0 \rightarrow |(Q\bar{Q})[(1^1S_0^{(8)}), (1^3S_1^{(8)})]g\rangle + Q\bar{Q}$ by at least an order of magnitude for the production of ψ_Q , h_Q and χ_{QJ} , while at the B factory $e^+e^- \rightarrow \gamma^* \rightarrow |(Q\bar{Q})[1^1S_0^{(8)}]g\rangle + g$ gives a significant contribution:

$$\frac{\sigma(e^+e^- \rightarrow \gamma^* \rightarrow |(c\bar{c})[(1^1S_0^{(8)})]g\rangle + g \rightarrow J/\psi + g)}{\sigma(e^+e^- \rightarrow \gamma^* \rightarrow |(c\bar{c})[(1^3S_1^{(1)})]g\rangle + c\bar{c} \rightarrow J/\psi + c\bar{c})} \sim 30\%.$$

2. Differential cross sections for the octet channels

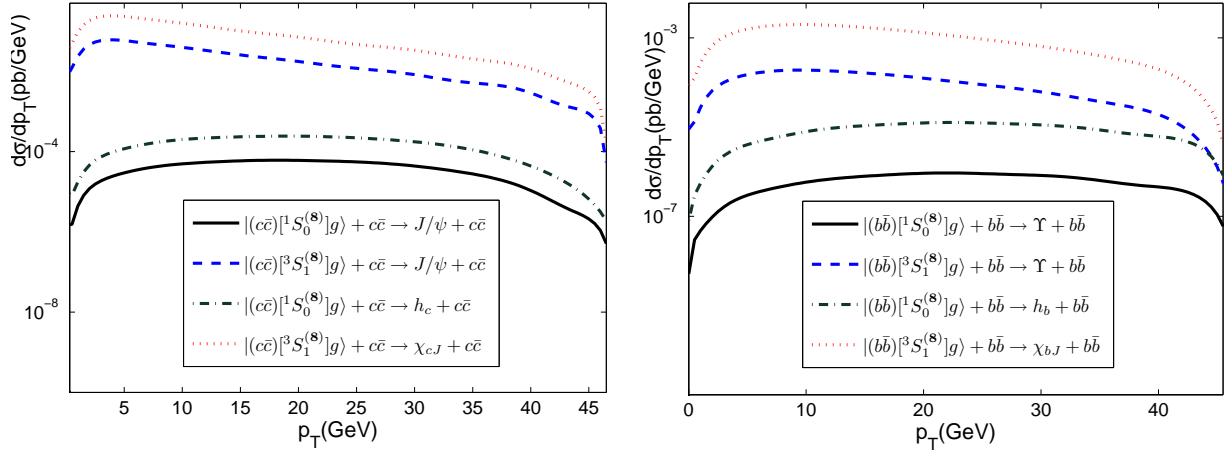


FIG. 15: The charmonium (left) and bottomonium (right) p_T distributions for the production processes $e^+e^- \rightarrow Z^0 \rightarrow |(Q\bar{Q})[(1^1S_0^{(8)}), (1^3S_1^{(8)})]g\rangle + Q\bar{Q} \rightarrow (\psi_Q, h_Q, \chi_{QJ}) + Q\bar{Q}$ at the collision energy $E_{cm} = m_Z$.

To better illustrate the relative importance of different production channels, we present the p_T and y distributions for the octet production channels of J/ψ , Υ , h_c , h_b , χ_{cJ} and χ_{bJ} in Figs. 15 and 16. Furthermore, the total cross sections with different p_T and y cuts are reported in Tables XIV and XV. The results show that the channel $e^+e^- \rightarrow Z^0 \rightarrow |(Q\bar{Q})[(1^3S_1^{(8)})]g\rangle + Q\bar{Q}$ will lead to a peak in the low p_T region at about 5 GeV for charmonium and 10 GeV for bottomonium.

Finally, we present the charmonium and bottomonium p_T distributions with various y cuts and the y distributions with various p_T cuts for the channel $e^+e^- \rightarrow Z^0 \rightarrow |H_Q\rangle + Q\bar{Q}$ in Figs. 17, 18, 19 and 20. In these figures, both color-singlet and color-octet contributions are included. Here, for the ψ_Q production through $e^+e^- \rightarrow Z^0 \rightarrow \psi_Q + Q\bar{Q}$, the components $|(Q\bar{Q})[(1^1S_0^{(8)})]g\rangle$, $|(Q\bar{Q})[(1^3S_1^{(8)})]g\rangle$ and $|(Q\bar{Q})[(1^3S_1^{(1)})]g\rangle$ have been summed up. For the P -wave quarkonium production through $e^+e^- \rightarrow Z^0 \rightarrow (h_Q, \chi_{QJ}) + Q\bar{Q}$, the contributions to h_Q and χ_{QJ} production, including both color-singlet and color-octet components, have been summed up.

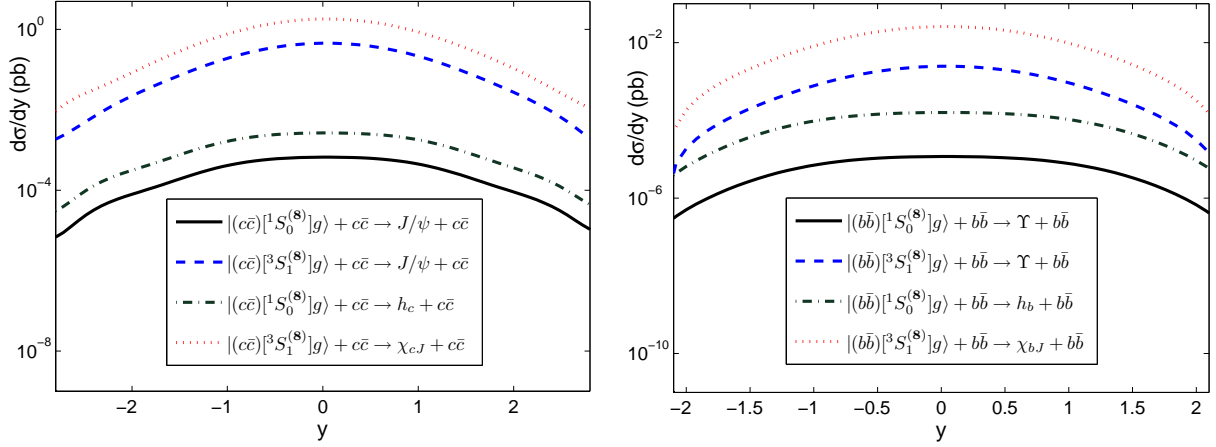


FIG. 16: The charmonium (left) and bottomonium (right) y distributions for the production processes $e^+e^- \rightarrow Z^0 \rightarrow |(Q\bar{Q})[({}^1S_0^{(8)}), ({}^3S_1^{(8)})]g\rangle + Q\bar{Q} \rightarrow (\psi_Q, h_Q, \chi_{QJ}) + Q\bar{Q}$ at the collision energy $E_{cm} = m_Z$.

Channel	$p_T > 5$ GeV	$p_T > 10$ GeV	$p_T > 15$ GeV
$\sigma(e^+e^- \rightarrow Z^0 \rightarrow (c\bar{c})[({}^1S_0^{(8)})]g\rangle + c\bar{c} \rightarrow J/\psi + c\bar{c})$	1.62×10^{-3} (96%)	1.41×10^{-3} (83%)	1.13×10^{-3} (67%)
$\sigma(e^+e^- \rightarrow Z^0 \rightarrow (c\bar{c})[({}^3S_1^{(8)})]g\rangle + c\bar{c} \rightarrow J/\psi + c\bar{c})$	6.80×10^{-1} (75%)	4.41×10^{-1} (48%)	2.85×10^{-1} (31%)
$\sigma(e^+e^- \rightarrow Z^0 \rightarrow (c\bar{c})[({}^1S_0^{(8)})]g\rangle + c\bar{c} \rightarrow h_c + c\bar{c})$	6.50×10^{-3} (96%)	5.65×10^{-3} (83%)	4.54×10^{-3} (67%)
$\sigma(e^+e^- \rightarrow Z^0 \rightarrow (c\bar{c})[({}^3S_1^{(8)})]g\rangle + c\bar{c} \rightarrow \chi_{cJ} + c\bar{c})$	2.72 (75%)	1.76 (48%)	1.14 (31%)
$\sigma(e^+e^- \rightarrow Z^0 \rightarrow (b\bar{b})[({}^1S_0^{(8)})]g\rangle + b\bar{b} \rightarrow \Upsilon + b\bar{b})$	2.69×10^{-5} (97%)	2.46×10^{-5} (89%)	2.11×10^{-5} (76%)
$\sigma(e^+e^- \rightarrow Z^0 \rightarrow (b\bar{b})[({}^3S_1^{(8)})]g\rangle + b\bar{b} \rightarrow \Upsilon + b\bar{b})$	3.80×10^{-3} (90%)	2.90×10^{-3} (69%)	2.02×10^{-3} (48%)
$\sigma(e^+e^- \rightarrow Z^0 \rightarrow (b\bar{b})[({}^1S_0^{(8)})]g\rangle + b\bar{b} \rightarrow h_b + b\bar{b})$	3.66×10^{-4} (97%)	3.34×10^{-4} (89%)	2.87×10^{-4} (76%)
$\sigma(e^+e^- \rightarrow Z^0 \rightarrow (b\bar{b})[({}^3S_1^{(8)})]g\rangle + b\bar{b} \rightarrow \chi_{bJ} + b\bar{b})$	3.99×10^{-2} (90%)	3.05×10^{-2} (69%)	2.12×10^{-2} (48%)

TABLE XIV: Total cross sections (in pb) for the octet channels of charmonium and bottomonium production via Z^0 propagator at the super Z factory with different p_T cuts, with $m_c=1.5$ GeV and $m_b=4.9$ GeV. The percentages in the parentheses represent the ratios between the cross sections with and without p_T cut.

IV. SUMMARY

In this paper, we have studied the charmonium and bottomonium production through the e^+e^- annihilation in the leading α_s -order. A detailed discussion on the heavy quarkonium production at the super Z factory via the two types of semi-exclusive channels, $e^+e^- \rightarrow |H_{Q\bar{Q}}\rangle + X$ with $X = Q\bar{Q}$ or gg , has been presented.

As usual, total cross sections are dominated by the color-singlet $1S$ -level quarkonium states. However the color-singlet quarkonium states at the $2S$ -level and the $1P$ -level, and the color-octet quarkonium state $|(Q\bar{Q})[{}^3S_1^{(8)}]g\rangle$ can also provide sizable contributions. Total cross sections for the color-singlet channels versus the collision energy E_{cm} have been presented in Figs. 6, 7, 8 and 9. The curves for the color-octet S -wave states have the same shapes as for the corresponding color-singlet S -wave states. In the low collision energy region, the cross sections are dominated by the processes via the γ^* propagator (in agreement with observations at the B factories): the main contributions are around 6 – 20 GeV for charmonium production and 10 – 40 GeV for bottomonium production. Around the collision energy $E_{cm} = m_Z$, due to the Z^0 -boson resonance effect, the cross sections become much larger for the processes via the Z^0 propagator. Then, at even higher energies, the total cross section drops down logarithmically for all the processes. By varying E_{cm} within the range of $(1 \pm 3\%)m_Z$, the total cross sections for J/ψ and Υ production drop to about 17% of their peak values.

At the super Z factory, the heavy quarkonium production processes $e^+e^- \rightarrow |H_{Q\bar{Q}}\rangle + X$ are dominated by those via the Z^0 propagator. Compared to the quarkonium production at the B factories (at an energy of about 10.6 GeV), much higher cross sections for $e^+e^- \rightarrow |H_{Q\bar{Q}}\rangle + X$ are expected at the super Z factory and at the Giga Z program of the ILC.

For the luminosity $\mathcal{L} = 10^{34} \text{cm}^{-2} \text{s}^{-1}$ ($\simeq 10^5 \text{pb}^{-1}/\text{year}$ integrated over one year [64]) we expect the following

Channel	$ y < 0.5$	$ y < 1.0$	$ y < 1.5$
$\sigma(e^+e^- \rightarrow Z^0 \rightarrow (c\bar{c})[(1^1S_0^{(8)})]g) + c\bar{c} \rightarrow J/\psi + c\bar{c})$	6.45×10^{-4} (38%)	1.18×10^{-3} (70%)	1.49×10^{-3} (88%)
$\sigma(e^+e^- \rightarrow Z^0 \rightarrow (c\bar{c})[(1^3S_1^{(8)})]g) + c\bar{c} \rightarrow J/\psi + c\bar{c})$	4.26×10^{-1} (47%)	7.14×10^{-1} (78%)	8.48×10^{-1} (93%)
$\sigma(e^+e^- \rightarrow Z^0 \rightarrow (c\bar{c})[(1^1S_0^{(8)})]g) + c\bar{c} \rightarrow h_c + c\bar{c})$	2.59×10^{-3} (38%)	4.73×10^{-3} (70%)	5.98×10^{-3} (88%)
$\sigma(e^+e^- \rightarrow Z^0 \rightarrow (c\bar{c})[(1^3S_1^{(8)})]g) + c\bar{c} \rightarrow \chi_{cJ} + c\bar{c})$	1.71 (47%)	2.86 (78%)	3.40 (93%)
$\sigma(e^+e^- \rightarrow Z^0 \rightarrow (b\bar{b})[(1^1S_0^{(8)})]g) + b\bar{b} \rightarrow \Upsilon + b\bar{b})$	1.14×10^{-5} (41%)	2.07×10^{-5} (75%)	2.58×10^{-5} (93%)
$\sigma(e^+e^- \rightarrow Z^0 \rightarrow (b\bar{b})[(1^3S_1^{(8)})]g) + b\bar{b} \rightarrow \Upsilon + b\bar{b})$	2.27×10^{-3} (54%)	3.63×10^{-3} (86%)	4.13×10^{-3} (98%)
$\sigma(e^+e^- \rightarrow Z^0 \rightarrow (b\bar{b})[(1^1S_0^{(8)})]g) + b\bar{b} \rightarrow h_b + b\bar{b})$	1.55×10^{-4} (41%)	2.81×10^{-4} (75%)	3.51×10^{-4} (93%)
$\sigma(e^+e^- \rightarrow Z^0 \rightarrow (b\bar{b})[(1^3S_1^{(8)})]g) + b\bar{b} \rightarrow \chi_{bJ} + b\bar{b})$	2.38×10^{-2} (54%)	3.81×10^{-2} (86%)	4.33×10^{-2} (98%)

TABLE XV: Total cross sections (in pb) for the octet channels of charmonium and bottomonium production via Z^0 propagator at the super Z factory with different y cuts, with $m_c=1.5$ GeV and $m_b=4.9$ GeV. The percentages in the parentheses represent the ratios between the cross sections with and without rapidity cut.

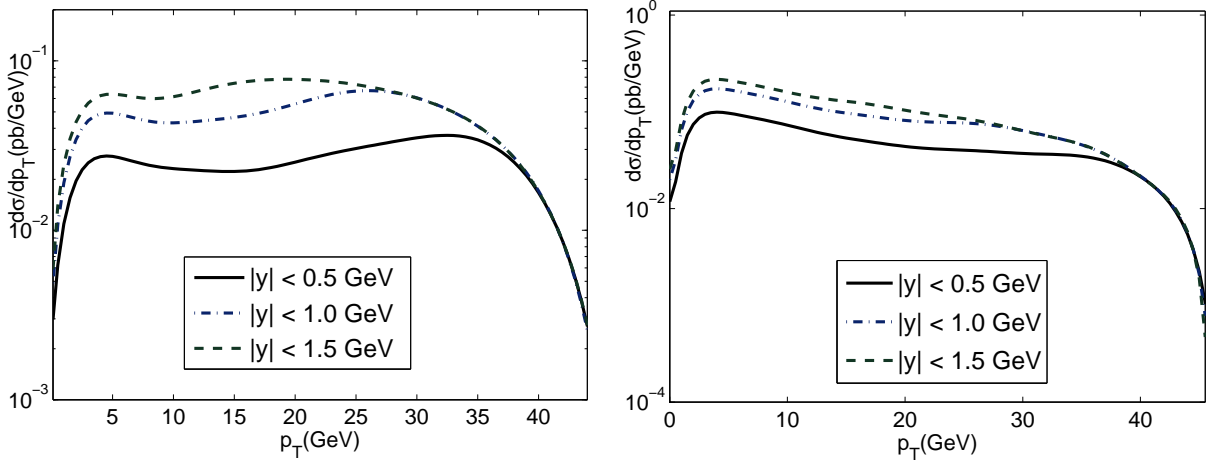


FIG. 17: The charmonium p_T distributions (left: J/ψ , right: P -wave charmonium) with various y cuts for $E_{cm} = m_Z$ and $m_c = 1.5$ GeV.

quarkonium yields per year:

$$\begin{aligned}
N_{J/\psi} &= 2.74 \times 10^5, N_{\psi'} = 1.16 \times 10^5, N_{\eta_c} = 1.76 \times 10^5, \\
N_{\eta'_c} &= 1.11 \times 10^5, N_{h_c} = 2.41 \times 10^4, N_{\chi_{c0}} = 7.37 \times 10^4, \\
N_{\chi_{c1}} &= 1.55 \times 10^5, N_{\chi_{c2}} = 2.17 \times 10^5
\end{aligned}$$

for the process $e^+e^- \rightarrow |H_{c\bar{c}}\rangle + c\bar{c}$ and

$$\begin{aligned}
N_{J/\psi} &= 3.91 \times 10^3, N_{\psi'} = 2.47 \times 10^3, N_{\eta_c} = 1.72 \times 10^4, \\
N_{\eta'_c} &= 1.09 \times 10^4
\end{aligned}$$

for the process $e^+e^- \rightarrow |H_{c\bar{c}}\rangle + gg$. For the bottomonium production we expect

$$\begin{aligned}
N_{\Upsilon} &= 2.22 \times 10^4, N_{\Upsilon'} = 1.08 \times 10^4, N_{\eta_b} = 1.94 \times 10^4, \\
N_{\eta'_b} &= 9.60 \times 10^3, N_{h_b} = 7.22 \times 10^2, N_{\chi_{b0}} = 1.58 \times 10^3, \\
N_{\chi_{b1}} &= 2.52 \times 10^3, N_{\chi_{b2}} = 2.90 \times 10^2
\end{aligned}$$

for the process $e^+e^- \rightarrow |H_{b\bar{b}}\rangle + b\bar{b}$ and

$$\begin{aligned}
N_{\Upsilon} &= 6.55 \times 10^3, N_{\Upsilon'} = 3.24 \times 10^3, N_{\eta_b} = 8.18 \times 10^3, \\
N_{\eta'_b} &= 4.05 \times 10^3
\end{aligned}$$

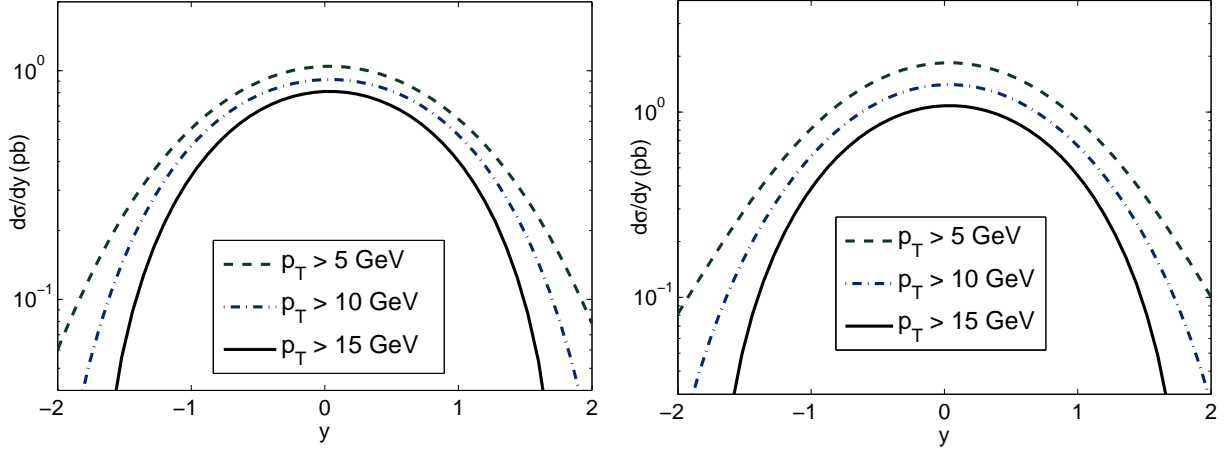


FIG. 18: The charmonium y distributions (left: J/ψ , right: P -wave charmonium) with various p_T cuts for $E_{cm} = m_Z$ and $m_c = 1.5$ GeV.

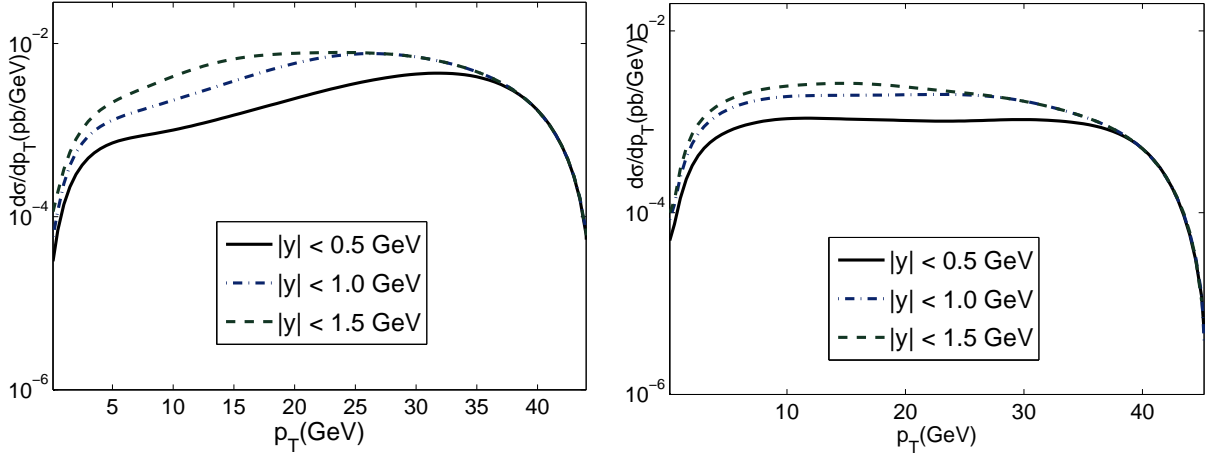


FIG. 19: The bottomonium p_T distributions (left: Υ , right: P -wave bottomonium) with various y cuts for $E_{cm} = m_Z$ and $m_b = 4.9$ GeV.

for the process $e^+e^- \rightarrow |H_{b\bar{b}}\rangle + gg$.

These numbers show that the super Z factory will represent an excellent platform for studying the heavy quarkonium properties, complementing those performed at the B factories BaBar and Belle and at the hadronic colliders Tevatron and LHC. To compare with the conventionally measured data on the prompt J/ψ or η_c (ψ_b or η_b) production, we need to consider the feeddown contributions from all the higher charmonium (bottomonium) states. These merging contributions can be done by using our present results for each state with the help of the measured branching ratios [47] as $\mathcal{B}[\psi(2s) \rightarrow J/\psi]$, $\mathcal{B}(\chi_{cJ} \rightarrow J/\psi)$, and etc..

For the charmonium and bottomonium production channels via the Z^0 propagator, there is approximate ‘‘spin degeneracy’’. Taking the charmonium production channels as an example, we obtain

$$\frac{\sigma_{e^+e^- \rightarrow Z^0 \rightarrow \eta_c + c\bar{c}}}{\sigma_{e^+e^- \rightarrow Z^0 \rightarrow J/\psi + c\bar{c}}} \simeq 96\%$$

and

$$\frac{\sigma_{e^+e^- \rightarrow Z^0 \rightarrow \chi_{c0} + c\bar{c}}}{\sigma_{e^+e^- \rightarrow Z^0 \rightarrow \chi_{c1} + c\bar{c}}} \simeq 91\%.$$

Such ‘‘spin degeneracy’’ is confirmed by analyzing the quarkonium p_T - and y - distributions, and also by a cross check using the fragmentation approach.

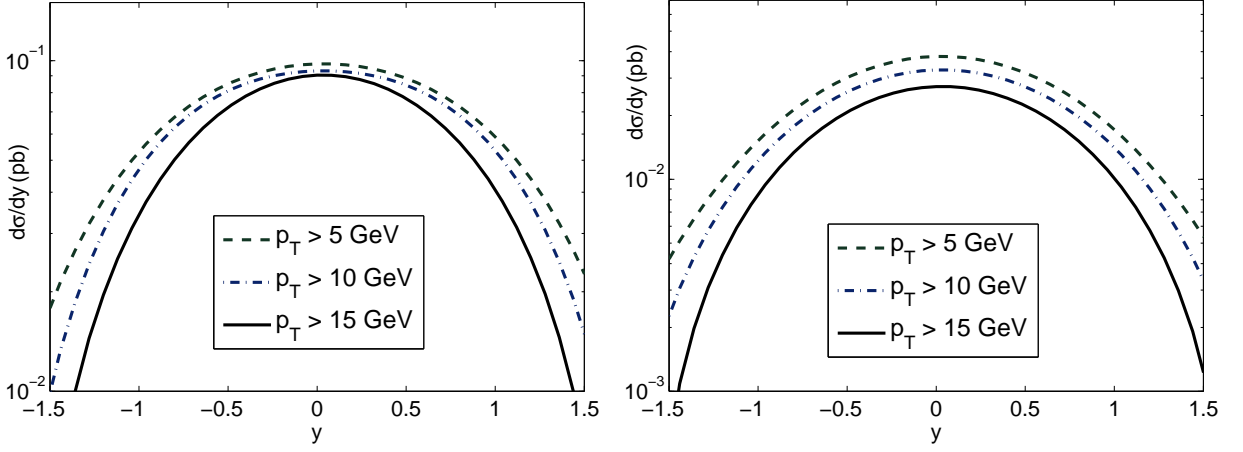


FIG. 20: The bottomonium y distributions (left: Υ , right: P -wave bottomonium) with various p_t cuts for $E_{cm} = m_Z$ and $m_b = 4.9$ GeV.

We have also discussed the uncertainties related to the knowledge of the effective quark masses. For the charmonium production channel $e^+e^- \rightarrow Z^0 \rightarrow |H_{c\bar{c}}\rangle + X$, when $X = c\bar{c}$, the uncertainties associated to the variation $m_c = 1.50 \pm 0.15$ GeV are $\sim 40\%$ for the S -wave case, and $\sim 70\%$ for the P -wave case; when $X = gg$, the uncertainties for both the S -wave and P -wave cases are $\sim 15\% - 19\%$. For the bottomonium production channel $e^+e^- \rightarrow Z^0 \rightarrow |H_{b\bar{b}}\rangle + X$, when $X = b\bar{b}$, the uncertainties caused associated to the variation $m_b = 4.90 \pm 0.15$ GeV are $\sim 11\%$ for the S -wave case, and $\sim 15\% - 18\%$ for the P -wave case; when $X = gg$, the uncertainties for both the S -wave and P -wave cases are $\sim 6\%$. To reduce the theoretical uncertainties on the predictions for the super Z factory, it will be important to perform a next-to-leading-order calculation for the channel $e^+e^- \rightarrow Z^0 \rightarrow |H_{c\bar{c}}\rangle + X$, which is in progress.

V. ACKNOWLEDGMENTS

This work was supported in part by the Fundamental Research Funds for the Central Universities under Grant No. CDJXS12300004 and CQDXWL-2012-Z002, the Program for New Century Excellent Talents in University under Grant No. NCET-10-0882, and the Natural Science Foundation of China under Grant No. 11075225 and No. 11275280. The authors are grateful for the anonymous referee's comments and suggestions that substantially improve the paper.

Appendix A: Phase space splitting for the color-singlet case

Generally, we can factorize the $2 \rightarrow 3$ phase into two parts

$$\begin{aligned}
 & d\Phi_3(p_1 + p_2; p_3, p_4, p_5) \\
 &= (2\pi)^4 \delta^{(4)}\left(p_1 + p_2 - \sum_{i=3}^5 p_i\right) \prod_{j=3}^5 \frac{d^3 p_j}{(2\pi)^3 2E_j} \\
 &= d\Phi_2(q; p_1, p_2) \frac{dq^2}{2\pi} d\Phi_3(q; p_3, p_4, p_5),
 \end{aligned} \tag{A1}$$

where $q^2 = (\sum_{i=3}^5 E_i)^2 - |\sum_{i=3}^5 \vec{p}_i|^2$ with $p_i = (E_i, \vec{p}_i)$. At the same time, the hard scattering amplitude can be rewritten as

$$\begin{aligned}
 & |\mathcal{M}_{2 \rightarrow 3}|^2 \\
 &= \left| \mathcal{M}_{2 \rightarrow 1}^\mu \left(-g_{\mu\nu} + \frac{q_\mu q_\nu}{M_Z^2} \right) \mathcal{M}_{1 \rightarrow 3}^\nu \right|^2 \\
 &= \left| \sum_\lambda \mathcal{M}_{2 \rightarrow 1}^\mu \mathcal{M}_{1 \rightarrow 3}^\nu \epsilon_\mu^*(q, \lambda) \epsilon_\nu(q, \lambda) \right|^2
 \end{aligned}$$

$$= \frac{1}{3} \sum_{\lambda_1, \lambda_2} |\mathcal{M}_{2 \rightarrow 1}^\mu \epsilon_\mu^*(q, \lambda_1)|^2 |\mathcal{M}_{1 \rightarrow 3}^\nu \epsilon_\nu(q, \lambda_2)|^2, \quad (\text{A2})$$

where $\epsilon(q, \lambda)$ stands for the Z^0 polarization vector. Then the process $e^+e^- \rightarrow |H_{cc}\rangle + c\bar{c}$ can be divided into two parts: the $2 \rightarrow 1$ process ($e^+e^- \rightarrow Z^0$) and the $1 \rightarrow 3$ process ($Z^0 \rightarrow |H_{Q\bar{Q}}\rangle + Q\bar{Q}$). The phase space of the $2 \rightarrow 1$ process is easily calculable, while for the $1 \rightarrow 3$ process it is the same as for the Z^0 decay into three final particles.

-
- [1] J.J. Aubert et al., Phys. Rev. Lett. **33**, 1404 (1974); J.E. Augustin et al., Phys. Rev. Lett. **33**, 1406 (1974).
[2] C.H. Chang, Nucl. Phys. B**172**, 425 (1980)
[3] T. Appelquist and H.D. Politzer, Phys. Rev. Lett. **34**, 43 (1975); A. De Rujula and S.L. Glashow, Phys. Rev. Lett. **34**, 46 (1975); C.A. Dominguez and M. Greco, Lett. Nuovo Cim. **12**, 439 (1975).
[4] J.H. Kuhn, J. Kaplan, E.G.O. Safiani, Nucl. Phys. B **157**, 125 (1979); W.Y. Keung, Phys. Rev. D **23**, 2072 (1981); J.H. Kuhn, H. Schneider, Phys. Rev. D **24**, 2996 (1981); J.H. Kuhn, H. Schneider, Z. Phys. C **11**, 263 (1981); L. Clavelli, Phys. Rev. D **26**, 1610 (1982).
[5] K. Hagiwara, A.D. Martin, W.J. Stirling, Phys. Lett. B **267**, 527 (1991); V.M. Driesen, J.H. Kuhn, E. Mirkes, Phys. Rev. D **49**, 3197 (1994).
[6] V.V. Kiselev, A.K. Likhoded, M.V. Shevlyagin, Phys. Lett. B **332**, 411 (1994).
[7] P.L. Cho, A.K. Leibovich, Phys. Rev. D **54**, 6690 (1996).
[8] E. Braaten, Y.Q. Chen, Phys. Rev. Lett. **76**, 730 (1996).
[9] F. Yuan, C.F. Qiao, K.T. Chao, Phys. Rev. D **56**, 321 (1997).
[10] C.H. Chang, C.F. Qiao, J.X. Wang, Phys. Rev. D **57**, 4035 (1998).
[11] K.Y. Liu, Z.G. He, K.T. Chao, Phys. Rev. D **69**, 094027 (2004).
[12] N. Brambilla, *et al.*, Quarkonium Working Group, arXiv: 0412158; Eur. Phys. J. C **71**, 1534 (2011).
[13] G. Aarons et al. (ILC Collaboration), International Linear Collider Reference Design Report 2 Physics at the ILC (2007).
[14] J. Erler S. Heinemeyerb, W. Hollikc, G. Weigleind, P.M. Zerwasb, Phys. Lett. B **486**, 125 (2000).
[15] J.P. Ma and Z.X. Zhang (The super Z-factory group), Sci. China: Phys., Mech. Astron. **53**, 1947 (2010).
[16] G.T. Bodwin, E. Braaten and G.P. Lepage, Phys. Rev. D **51**, 1125 (1995).
[17] F. Abe et al., CDF Collaboration, Phys. Rev. Lett. **79**, 572 (1997); Phys. Rev. Lett. **79**, 578 (1997).
[18] E. Braaten and S. Fleming, Phys. Rev. Lett. **74**, 3327 (1995).
[19] P. Cho and M. Wise, Phys. Lett. B**346**, 129 (1995).
[20] T. Affolder, *et al.*, CDF Collaboration, Phys.Rev. Lett.**85**, 2886 (2000).
[21] A. Abulencia *etal.*, CDF collaboration, Phys. Rev. Lett. **99**, 132001 (2007).
[22] B. Abelev *etal.*, ALICE Collaboration, Phys. rev. Lett. **108**, 082001 (2012).
[23] K.Y. Liu, J.P. Ma and X.G. Wu, Phys. Lett. B**645**, 180 (2007); X.G. Wu and Z.Y. Fang, Phys. Rev. D**80**, 034010 (2009).
[24] M. Cacciari, M. Greco, M.L. Mangano and A. Petrelli, Phys. Lett. B **356**, 553 (1995); E. Braaten and T.C. Yuan, Phys. Rev. D **52**, 6627 (1995).
[25] M. Cacciari and M. Kramer, Phys. Rev. Lett. **76**, 4128 (1996).
[26] M. Beneke and I.Z. Rothstein, Phys. Rev. D **54**, 2005 (1996).
[27] M. Beneke and M. Kramer, Report No. CERN-TH/96-310.
[28] M. A. Sanchis-Lozano and B. Cano-Coloma, Nucl. Phys. Proc. Suppl. **55A**, 277 (1997).
[29] X.G. Wu, C.H. Chang, Y.Q. Chen, Z.Y. Fang, Phys. Rev. D**67**, 094001 (2003).
[30] Y.J. Zhang, Y.Q. Ma, K. Wang and K.T. Chao, Phys. Rev. D**81**, 034015 (2010).
[31] Y.Q. Ma, K. Wang and K.T. Chao, Phys. Rev. Lett. **106**, 042002 (2011).
[32] M. Butenschon and B.A. Kniehl, Phys. Rev. Lett. **106**, 022003 (2011).
[33] L.D. Landau, Dokl. Akad. Nauk SSSR **60**, 207 (1948); I.Ya. Pomeranchuk, Dokl. Akad. SSSR **60**, 263 (1948); C.N. Yang, Phys. Rev. **77**, 55 (1950).
[34] K. Cheung, W.Y. Keung, T.C. Yuan, Phys. Rev. Lett. **76**, 877 (1996).
[35] L.C. Deng, X.G. Wu, Z. Yang, Z.Y. Fang and Q.L. Liao, Eur. Phys. J. C**70**, 113 (2010).
[36] Z. Yang, X.G. Wu, L.C. Deng, J.W. Zhang and G. Chen, Eur. Phys. J. C**71**, 1563 (2011).
[37] C.F. Qiao, L.P. Sun and R.L. Zhu, JHEP **1108**, 131 (2011).
[38] Z. Yang, X.G. Wu, G. Chen, Q.L. Liao and J.W. Zhang, Phys. Rev. D**85**, 094015 (2012).
[39] C.H. Chang, J.X. Wang and X.G. Wu, Sci. China: Phys., Mech. Astron. **53**, 2031 (2010); arXiv:1005.4723.
[40] J. Jiang, X.G. Wu, Q.L. Liao, X.C. Zheng and Z.Y. Fang, Phys. Rev. D **86**, 054021 (2012).
[41] A. Petrelli, M. Cacciari, M. Greco, F. Maltoni, M.L. Mangano, Nucl. Phys. B **514**, 245 (1998).
[42] R. Kleiss and W. J. Stirling, Comput. Phys. Commun. **40**, 359 (1986).
[43] G.P. Lepage, J. Comput. Phys. **27**, 192 (1978).
[44] C.H. Chang, J.X. Wang and X.G. Wu, Comput. Phys. Commun.**177**, 467 (2007); C.H. Chang, J.X. Wang and X.G. Wu, Comput. Phys. Commun.**181**, 1144 (2010); X.Y. Wang and X.G. Wu, Comput. Phys. Commun. **184**, 1070 (2013).
[45] C.H. Chang, C. Driouch, P. Eerola, and X.G. Wu, Comput. Phys. Commun. **159**, 192 (2004); C.H. Chang, J.X. Wang, and X.G. Wu, Comput. Phys. Commun. **174**, 241 (2006); 175, 624 (2006); X.Y. Wang and X.G. Wu, Comput. Phys.

- Commun. **183**, 442 (2012).
- [46] P. Cho, A.K. Leibovich, Phys. Rev. D **53**, 150 (1996); P. Cho, A.K. Leibovich, Phys. Rev. D **53**, 6203 (1996).
 - [47] J. Beringer *et al.*, (Particle Data Group), Phys. Rev. D **86**, 010001 (2012).
 - [48] J.D. Bjorken, Phys. Rev. D **17**, 171 (1978).
 - [49] M. Suzuki, Phys. Lett. B **71**, 139 (1977).
 - [50] S.J. Brodsky, C. Peterson, and N. Sakai, Phys. Rev. D **23**, 2745 (1981).
 - [51] C. Peterson, D. Schlatter, I. Schmitt, and P.M. Zerwas, Phys. Rev. D **27**, 105 (1983).
 - [52] L. Clavelli, Phys. Rev. D **26**, 1610 (1982).
 - [53] C.R. Ji and F. Amiri, Phys. Rev. D **35**, 3318 (1987).
 - [54] C.R. Ji and F. Amiri, Phys. Lett. B **195**, 593 (1987).
 - [55] E. Braaten, T.C. Yuan, Phys. Rev. Lett. **71**, 1673 (1993).
 - [56] C.H. Chang and Y.Q. Chen, Phys. Rev. D **46**, 3845 (1992).
 - [57] E. Braaten, K. Cheung, and T.C. Yuan, Phys. Rev. D **48**, R5049 (1993).
 - [58] E. Braaten, K. Cheung, and T.C. Yuan, Phys. Rev. D **48**, 4230 (1993).
 - [59] M. Suzuki, Phys. Rev. D **33**, 676 (1986).
 - [60] T.C. Yuan, Phys. Rev. D **50**, 5664 (1994).
 - [61] M. Cacciari, M. Greco and P. Nason, JHEP **9805**, 007 (1998).
 - [62] M. Cacciari and P. Nason, Phys. Rev. Lett. **89**, 122003 (2002).
 - [63] S.J. Brodsky, X.G. Wu, Phys. Rev. Lett. **109**, 042002 (2012); S.J. Brodsky, X.G. Wu, Phys. Rev. D **85**, 034038 (2012); S.J. Brodsky, X.G. Wu, Phys. Rev. D **86**, 054018 (2012); S.J. Brodsky and L. Di Giustino, Phys. Rev. D **86**, 085026 (2012); M. Mojaza, S.J. Brodsky, X.G. Wu, Phys. Rev. Lett. **110**, 192001 (2013); X.G. Wu, S.J. Brodsky, M. Mojaza, arXiv:1302.0599;
 - [64] Tao Han, arXiv:0508097 [hep-ph].